CERN - SPSC- 89-73

ρ

EUROPEAN ORGANISATION FOR NUCLEAR RESEARCH

Letter of Intent

# Large Acceptance Hadron and Photon Detector for an Investigation of Pb-induced Reactions at the CERN SPS

Submitted to the SPSC by the NA35 and WA80 Collaborations

Athens Univ.
  A. Karabarbounis, A. Panagiotou, A. Petridis, G. Vassileiadis, J. Vassileiou

Bari Univ.
  M. Callichio, C. Favuzzi, E. Nappi, F. Posa, P. Spinelli

CERN
  J. Pfennig, F. Rohrbach

Cracow Inst.Nucl.Phys.
  J. Bartke, E. Gladysz, M. Kowalski

Darmstadt GSI
  R. Bock, R. Brockmann, B. Fleischmann, M. Fuchs, H. Gutbrod, B.W. Kolb, I. Lund,
  G. Paic, A. Sandoval, H.R. Schmidt

Frankfurt/Main Univ.
  J. Eschke, E. Hartig, W. Heck, S. Kabana, J. Kosiec, A. Kühmichel, M. Labanas, S. Margetis, R. Renfordt, D. Roehrich, I. Schneider, R. Stock, H. Stroebele, A. Thomas, S. Wenig

Freiburg Univ.
  J. Baechler, M. Hoffmann, K. Runge, E. Schmoetten

Groningen, KVI
H. Löhner

Lawrence Berkeley Lab.
J.W. Harris, P. Jacobs, G. Odyniec, A.M. Poskanzer, H.G. Pugh, W. Rauch,
H.G. Ritter, S. Tonse

Lund University
G. Claesson, A. Eklund, S. Garpman, H.A. Gustafsson, J. Idh, P. Kristiansson,
A. Oskarsson, I. Otterlund, S. Persson, E. Stenlund, K. Söderström

Marburg Univ.
R. Keidel, A. Pieper, F. Puehlhofer

München MPI
I. Derado, V. Eckardt, P. Freund, H.J. Gebauer, N. Schmitz, J. Seyboth, P. Seyboth,
J. Seyerlein, G. Vesztergombi

Münster University
M. Bahr, P. Beckmann, F. Berger, G. Clewing, L. Dragon, R. Glasow, G. Hölker,
K.H. Kampert, M. Purschke, T. Peitzmann, H. Rothgänger, R. Santo, R. Schmidt,
K. Steffens, D. Stüken

Oak Ridge National Laboratory
T.C. Awes, C. Baktash, R.L. Ferguson, I.Y. Lee, F.E. Obenshain, F. Plasil, S. Saini,
M. Tincknell, G.R. Young

University of Tennessee
A. Franz, S.P. Sorensen

VECC-BARC Calcutta
B. Sinha, Y.P. Viyogi

Warsaw Inst. Nucl. Studies
H. Bialkowska, T. Siemiarczuk

Warsaw Univ.
W. Dominik, M. Gazdzicki, E. Skrzypczak

Zagreb Rudjer Boskovic Inst.
P. Buncic, D. Ferenc, K. Kadija, A. Ljubicic, D. Vranic

Spokesmen: H.H. Gutbrod (WA80) and R. Stock (NA35)

# Contents

# Large Acceptance Hadron and Photon Detector for an Investigation of Pb-induced Reactions at the CERN SPS

Submitted to the SPSC by the NA35 and WA80 Collaborations

# 1 Physics Considerations

## 1.1 The Need for Heavy Nuclear Projectiles in the Search for the Quark-Gluon-Plasma State of Matter

Recent QCD calculations on extended lattices, which included dynamical $u$, $d$ and $s$ quarks[1] have reaffirmed the existence of a deconfined plasma state at an energy density of about 2.5–3 GeV/fm$^3$. They have also demonstrated the first order character of the phase transition between hadronic and quark matter. The guide-lines derived from such stationary-state calculations concerning suitable dynamical conditions, in nucleus-nucleus collisions, are obvious:

1. One has to create a transient state of substantial spatial extension, far exceeding the typical confinement volume of a few fm$^3$, and of a sufficiently high energy density.

2. Critical parameters, like the energy density and the baryochemical potential, should exhibit a smooth variation in all space-time directions.

3. The life-time has to be as long as possible. More precisely: the expansion time scale (volume doubling time) has to be slower than the scale on which quarks and gluons approach thermo-chemical equilibrium.

1

All these criteria have to be simultaneously fulfilled in order to create a transient plasma state, thus preventing a direct hadronization to occur from local, incoherent interaction subvolumes, resembling those of ordinary hadron-hadron collisions.

The first round of experiments with SPS beams of $^{16}O$ and $^{32}S$ has shown[2] that an energy density of the right magnitude, 2-3 GeV/fm$^3$, is in fact reached in central collisions of such projectiles with heavy target nuclei at 200 GeV/$N$. However, this may not be sufficient as illustrated by two simple considerations:

1. Oxygen and Sulfur nuclei offer an unfavourable surface-to-volume ratio. Projecting their nucleon density onto the reaction plane one finds an average transverse spacing between neighbours in excess of the confinement dimension of 1 fm. The reaction "strings" of individual microscopic nucleon-nucleon collisions, known from pion correlation studies to be of about 1 fm dimension[3], will thus not be forced to significantly interpenetrate. The local energy density will thus vary substantially in transverse direction, throughout the macroscopic reaction volume. With Pb projectiles the situation is reversed: with an average spacing of about 0.5fm most of the parallel N-N interaction zones will overlap creating a smooth energy density profile in transverse direction.

2. In comparing plasma Debeye-screening radii with the radii of various hadrons, Matsui and Satz[4] concluded that the *melting down* of all hadronic species inside a plasma occurs, not right at the critical temperature $T_c$ but at $T \approx 1.2T_c$. With $\epsilon \sim T^4$ this implies a range of desireable energy density up to about $2\epsilon_c$. This is outside the reach with light projectiles. Based on the results of present S+heavy nucleus studies, we may extrapolate to central Pb+Pb collisions[5]: an energy density of about 4-5 Gev/fm$^3$ should be created in the central sector, of about 6 fm diameter. This volume should thus satisfy all foreseeable demands, as outlined above.

We thus expect central Pb+Pb collisions at top SPS energy to offer qualitatively different dynamical conditions, leading to a set of clear-cut answers concerning the candidate signals

of plasma formation if such a state exists. We therefore propose a second generation experiment which will be designed to cope with the high multiplicity of produced particles, and to investigate various hadronic signals at the event-by-event level, in a mode which is as charged-particle-exclusive as possible. The focus on an analysis of macroscopic and microscopic observables, referring to the *individual events*, stems from our expectation that the phase transition, due to the statistical fluctuations in the collision dynamics, may not uniformly occur in the *average* central Pb+Pb collision.

## 1.2  Hadronic Signals of Plasma Formation

The proposed second generation detector system (to be described in the next section) attempts to stay as close to $4\pi$ coverage as possible, in line with our current NA35 and WA80 approach. The main new feature will be *hadron identification*, either track by track (for $\pi^{\pm}$, $K^{\pm}$, $p$, $\overline{p}$ and $e^{+}$, $e^{-}$, $\mu^{+}$, $\mu^{-}$) or after invariant mass reconstruction ($\pi^{0}$, $\eta$). Depending on an optional extension of the planned setup we intend to add neutral strange particle ($K_0$, $\Lambda$, $\overline{\Lambda}$) identification. The other, fundamentally new feature of the planned experiment is a consequence of the large volume tracking devices (that are required due to the very high spatial track density): we will identify about 600–1000 charged particles per central Pb+Pb collision event, enabling us to extract certain *collective event features* on an *event-by-event* basis. With those, we mean not the previously accessible integral quantities like event charged particle multiplicity, transverse energy, forward energy flow etc, but differential, non-trivial observables of individual events, such as

1. the pion *source* radii in transverse and longitudinal directions (from $2\pi^{-}$, $2\pi^{+}$ correlation);

2. the entropy produced in the reaction, as measured by the rapidity density and transverse momentum inverse slope (*temperature*) of the pions;

3. the baryon and antibaryon distributions in rapidity space.

3

Whereas the former, integral quantities lend themselves to online triggering – we will employ $E^T$ and $E$ ($\Theta \approx 0°$) in our experiment – the latter event features can not (and need not) be implemented in an on-line trigger. They follow from off-line, event by event analysis, which will result in subensembles characterized by e.g. large source radii, high *temperature* or $\langle p_T \rangle$, high *quark stopping* (high net baryon density near midrapidity). Such ensemble characteristics can then be cross-correlated with each other, as well as with strangeness yields, features of high statistics $p_T$ spectra, multiplicity distributions and fluctuations, etc., in the corresponding sub-ensembles.

Our basic aim is to select rare events from among the overall *central trigger* events. Individual hadronic signals (high strangeness abundance, low $J/\Psi$ yield etc.) provide necessary but not in themselves sufficient evidence for plasma formation. Candidate events should therefore be selected by cumulative criteria, i.e. by the simultaneous deviation of various observables from the normal final state of hadron interactions.

The minimum number of identified hadrons per event, required by this analysis of collective event features, is about 500–1000 as we shall illustrate below. For average central Pb+Pb collisions at $180 \, \text{GeV}/N$ (top SPS energy) one expects a total charge particle multiplicity of about 2500. Recalling the reflection symmetry about midrapidity in this reaction, the half-space $y \geq 2.9$ contains all the information. It is thus sufficient to cover the interval $2.9 < y < 4.5$ by tracking and particle identification – this does already imply large volume detectors.

The effect of ensemble selection is illustrated by recent NA35 results in Fig. 1. It shows the ratio of $\langle \Lambda \rangle / \langle h^{\pm} \rangle$ vs. the charged hadron multiplicity $h^{\pm}$ in the multiplicity domains corresponding to peripheral, intermediate and central S+S collisions at $200 \, \text{GeV}/N$. The $\langle \Lambda \rangle$ values refer to the domain $0.5 < y < 2.6$, $p_T > 0.50 \, \text{GeV}/c$. Central collision events have an enhanced strangeness content. After extrapolation to $4\pi$, $\langle \Lambda \rangle^{S+S}$ turns out to be $80 \pm 15$ times the $\langle \Lambda \rangle$ observed in $p+p$ at 205 GeV, whereas $\langle h^- \rangle^{S+S}$ is only $35 \pm 5$ times $\langle h^- \rangle^{pp}$, in the central collision subsample. A similar enhancement is observed for $\langle K_0^s \rangle$. Fig. 1 indicates that it would be very interesting to pursue the strange to nonstrange ratio

up to the $h^-$ in excess of 1000, expected for central Pb+Pb collisions -- irrespective of the question whether or not high strangeness content of the final state presents evidence for plasma formation[6]. We mention here the possibilities for di-lamda and/or *strangelet* formation in a 30% strangeness final state[7].

The *self analyzing* capacity of an experiment that identifies up to 1000 charged hadrons per event is further illustrated in Fig. 2 a,b,c. The 2-$\pi$ correlation in such a single event (Fig. 2a) is simulated by a Monte Carlo procedure. The input values, a source radius of 10 fm and a chaoticity parameter of $\lambda = 0.8$, are reproduced within about 10%. This is accurate enough in order to clearly separate two classes, with $\langle R \rangle = 10$ and 15 fm, respectively, at the event by event level. Fig. 2b shows the single event $p_T$ distributions for 800 pions in the interval $3 < y < 4.5$ assuming thermal sources of $T = 150$ and $200\,\mathrm{MeV}$, respectively. Again, the single event output clearly distinguishes the two cases. Finally, Fig. 2c shows the proton rapidity distribution, for a single central Pb+Pb collision event generated with FRITIOF. We observe, at the level of one event, the well known feature that the baryon number density of FRITIOF peaks *away* from midrapidity because of low stopping power. We would thus select for events that do exhibit *high* midrapidity baryon number.

After having stressed the selectivity of the proposed Large Acceptance Hadron Detector we turn now to a brief enumeration of the physics quantities that we want to extract from the analysis of properly selected ensembles of events.

1. Charged particle multiplicity, and rapidity distributions

Fig. 3 shows Fritiof simulation results for Pb+Pb collisions at $160\,\mathrm{GeV}/N$: minimum bias distributions of charged particle multiplicity and global transverse energy, as well as the density distribution in pseudorapidity of charged particles in central collisions. It has been suggested that fractal dimensions can be used to analyze the multiplicity of charged particles in different pseudo-rapidity windows[8,9]. A further motivation for the study of the multiplicity of charged particles locally as well as globally is that

5

it is related to the entropy density[10] which is extremely important in the context of a phase transition in nuclear matter.

To a large degree the shapes of the multiplicity and transverse energy distributions can be reproduced by treating the nucleus-nucleus collisions by a zero-order or geometrical approximation. The main task of ultrarelativistic ion physics is to separate and interpret those effects which go beyond the geometrical approximation[11]. The nuclear geometry must be well understood if one wants to achieve a correct separation of the non-linear effects containing the interesting dynamics. In Pb+Pb interactions high string densities are expected and interference phenomena might affect the radiation from the strings[12].

Fritiof model simulations for Pb+Pb show that the shape of the pseudorapidity distributions are very stable; the shape of the rapidity density distribution is the same in a central interaction as in an average minimum bias event. Will this stability be brooken because of strong non-linear effects in central events with high string densities?

The most straightforward approach for studying fluctuations is to look at the width of transverse energy and multiplicity distributions. Using data from $pp$ interactions it is possible to calculate the expected width from heavy ion collisions assuming independent nucleon-nucleon collisions and a suitable density distribution within the nuclei. Significant deviations from calculated widths may indicate a certain degree of non linear phenomena.

A marked difference between transverse energy and multiplicity is that the transverse energy is continous whereas multiplicity is a discrete quantity. When a limited rapidity window and the discreteness of the multiplicity are considered the stochastic nature of the sources will tend to increase the normalized variance in accordance with the formula[13]:

$$\Omega(y\Delta y) - (\Delta y \cdot \langle \rho(y) \rangle) - 1 = \text{constant}$$

6

$\Omega$ is the normalized variance and $\Delta y$ is the width of the rapidity interval under consideration. $\langle \rho \rangle$ is the mean of the density distribution in the interval $\Delta y$. The constant is determined from data. $\Omega$ can then be studied as a function of $y$ or $\Delta y$. Significant deviations from the formula are a sign of deviations from the stochastic assumptions. It would thus demand some additional coherent mechanisms to explain the deviations. This method requires that multiplicity is measured in a large $y$-interval.

For small $\Delta y$-windows a clear deviation from the formula above is observed in the data from the previous runs at CERN. These non-linear effects can be directly related to multi-particle correlations in general and Hanbury-Brown and Twiss interference in particular[14]. There are recent observations which indicate that additional effects are necessary to explain the observed deviations, i.e. effects related to fractal dimensions and chaos theory. In order to study the intermittent behaviour of these fluctuations, as proposed by Bialas and Peschanski[15], an extremely high spatial resolution is needed at least in a limited region. A large coverage permits studies of how the effect varies in different regions of phase space.

2. Rapidity distribution of $\pi^{\pm}$, $K^{\pm}$, $p$, $\bar{p}$ in $3 < y < 4.5$

For identified hadrons, the measurement of the domain $3 < y < 4.5$ is representative of the entire interval $1.5 < y < 4.5$ because of reflection symmetry in Pb+Pb collisions. The ratio

$$R^{\pi/K}(y) = \frac{\mathrm{d}N(\pi)/\mathrm{d}y}{\mathrm{d}N(K)/\mathrm{d}y}$$

will yield information on the relative $s,\bar{s}$ to $ud/\bar{u}\bar{d}$ concentration as a function of rapidity. It will help answering the question whether the relative strangeness concentration follows the energy density or the net baryon number density, the latter obtained as

7

$$D^B(y) = \frac{N+Z}{Z} \cdot \frac{dN(p) - dN(\bar{p})}{dy} + \frac{dN(\Lambda) - dN(\bar{\Lambda})}{dy} .$$

This quantity also gives information about the valence quark final state distribution and, thus, about the stopping power for quarks, in distinction to the stopping power for energy, as revealed to first order by the sum-total of pion and kaon $y$-distributions.

3. Charged hadron transverse momentum/energy spectra

Besides clarifying the question whether we get a fraction of events exhibiting the extremely flat $p_T$ distribution shape reported for JACEE cosmic ray results[16], obtained at yet higher energies, the detailed shape of $p_T$ distributions for $\pi$, $K$, $p$ has been recently discussed in terms of an isentropic radial expansion mechanism by Lee and Heinz[17]. A transient plasma state would change the expansion time scale and leave its fingerprints in a difference of $K^+$ and $K^-$ spectra, as well as in other detailed features. This observable requires high statistics data in the $0 < p_T < 1.5\,\text{GeV/c}$ domain.

4. Two-pion and multi-pion Bose-Einstein-correlation

Fig. 4 shows a calculation by Zajc[18] for a final state containing 500 like-sign pions in configuration space ($\Theta$ polar, $\phi$ azimuthal CM emission angle). The clustering, due to Bose-Einstein correlation, is obvious and constitutes the most striking feature of a 1000-particle final state. Only the two-$\pi$ correlation aspect has been comprehensively analyzed in the present round of O, S induced reactions[19]. Extending this analysis to Pb+Pb collisions (and much higher statistical precision) we intend to investigate the 4-dimensional space-time source structure. It is an open question whether it should react sensitively to the existence, or non-existence, of a transient plasma phase[20].

It is intuitively clear, furthermore, that a multiparticle clustering of the distinctness offered by Fig. 4 must be analyzeable in terms of a more macroscopic description

which emphasizes the multi-particle aspect rather than the two pion yield enhancement at $\Delta p \rightarrow 0$. Theoretical development in this direction has just begun[14].

5. Two-Kaon Bose-Einstein correlations

The proposed experiment will identify at least about 30 $K^+$ and about 15 $K^-$ per event, in the $3 < y < 4.5$ interval, leading to excellent statistics already in sub-samples of about 50.000 events ($2 \cdot 10^7 K^+$ pairs, $5 \cdot 10^6 K^-$ pairs!). The $K^+$ and $K^-$ correlations should reflect different aspects of the expansion and freezeout mechanism, both between themselves, and also relative to the pion correlations[19].

6. Strangeness in the final state from $K^\pm$ and $\Lambda$, $\overline{\Lambda}$, $K_0$ measurement

According to Kogut and Sinclair's lattice QCD calculation[1] the plasma contains the fractions $[u, \overline{u}, d, \overline{d}]$, $[s, \overline{s}]$ and $[gluons]$ in the ratio $4 : 1 : 5$. In the limiting (unlikely) case that hadronization of the gluonic energy fraction occurs with the same $4 : 1$ ratio, the maximum final state strangeness abundance could be about 25% (before $\eta$ and $\Sigma^\pm$ decay). It has been speculated that such a concentration of strangeness could give rise to exotic strange object formation[7] if there occured an *unmixing* of $s$ from $\overline{s}$ quarks, as expected for a mixed-phase plasma/hadronic matter expansion. Without attaching too much weight to this far-out speculation we will look for low charge-to-mass objects in the final state.

We will estimate the strangeness concentration by measuring the $\langle K^+ \rangle$, $\langle K^- \rangle$ per event and, in a considered extension of the experiment (see sect. 3), the $K_0$, $\Lambda$ and $\overline{\Lambda}$ multiplicities. The rank of the strangeness concentration as a diagnostic tool for plasma formation is still under intense theoretical discussion, with an indication of consensus toward the statement that high concentration is a *necessary* condition for plasma formation, and that it is hard to imagine how a reaction dynamics *without* a transient plasma state could reach saturation strangeness concentration[21].

9

## 7. Neutral pions and etas

The proposed experiment will identify neutral pions, etas and perhaps heavier mesons by means of their two-photon decays. This is difficult to do on an event-by-event basis, in contrast to the situation for charged pions and kaons and also for protons, as two final-state particles (in this case photons) must be reconstructed, and the resulting combinatorial backgrounds dealt with. Even so, it is possible to study the properties of these particles for different classes of events, to be selected according to TPC event by event information regarding pion correlation, strangeness content, transverse momentum spectrum, etc.. Given the high reconstruction efficiency of the photon detectors at high $p_T$, it is possible to study these particles over a large $p_T$ range. One would look for evidence of hydrodynamic flow, which should manifest itself in $p_T$ distributions which again differ from those of charged kaons mentioned above. At higher $p_T$ the role played by the "Cronin-effect" in central Pb+Pb collisions can be studied.

The slope parameter of the $p_T$ distribution of $\pi^0$ has already been observed to saturate as a function of normalized particle density[22]. By using lead projectiles one will have a much larger reach in this variable, much as one will in energy density, so that whether a "plateau+rise" behavior exists as suggested by Van Hove[23] can be studied. One also can investigate out to rather large values of $p_T$ (in excess of 3 GeV/c as already seen in O+Au data of WA80) so that contact to hard scattering and perturbative $QCD$, but in this case for nuclei+nuclei, can be made.

The $\eta$ meson carries strangeness via its quark content of $\eta = \frac{1}{\sqrt{6}} \cdot (u\bar{u} + d\bar{d} - 2 \cdot s\bar{s})$. Unlike the kaons, both strange and anti-strange quarks are present, meaning the $\eta$ should be affected differently than kaons in any scheme involving dynamical strangeness separation.

## 1.3 Direct photons

Collisions of the quarks, anti-quarks and gluons can lead to emission of single, "direct" photons through two basic processes: $QCD$ Compton scattering and quark-antiquark annihilation. The number of such photons observed reflects the time-integral of all such photon emissions over the history of a collision. It is expected that creation of a deconfined phase should lead to a large increase in the proper time available (in both deconfined and mixed phases) for this emission to proceed, resulting in a marked increase in the yield of such photons.

These photons are expected to lie in the $p_T$ range from 1-4 times the critical temperature, i.e. for $p_T = 200$-$800 \, MeV/c$. Their spectral shape carries information on the nature of the emitting phase, with a power law reflecting emission from a thermalized phase. The exponent of this power law is related to the velocity of sound in the plasma phase. If the phase transition is first order, an exponential rise is also expected[24].

It was pointed out that the emission from a mixed phase can also be strongly enhanced due to the long proper time duration of a mixed phase[25,26]. This happens because a mixed phase has a zero velocity of sound, meaning a transverse rarefaction wave cannot propagate. In that case the longitudinal expansion is solely responsible for reducing the energy density in the mixed phase.

The yield is also suggested to depend on the square of the particle density in rapidity (which is a measure of entropy)[25]. This again suggests that the separation of events into classes, discussed earlier for other observables, is a necessary capability for this part of the study.

We are currently also investigating the usefulness of photon correlation analysis at the event by event level. This could proceed at the level of photon pairs and of pairs of identified $\pi^0$. The former could hope to observe any extended common source of (direct) photons. The latter will tie on to our HBT analysis of charged pion pairs.

The direct photon measurement necessarily relies on a correction of the measured in-

11

clusive photon yield for all known sources of non-direct, particularly decay photons. This places a premium on excellent invariant mass resolution and broad $p_T$ acceptance for the $\pi^0$ and $\eta$ mesons. This leads to the choice of a very high performance, highly segmented photon calorimeter to perform this task in the high multiplicity environment that will be encountered in Pb+Pb collisions.

# References

[1] J.B.Kogut and D.K.Sinclair, Phys.Rev.Lett. 60(1988)1250

[2] For a review, see H.G.Ritter, Nucl.Phys.A 488(1988)651C

[3] T.Akesson et al., Phys.Lett.B 187(1987)420

[4] T.Matsui and H.Satz, Phys.Lett.B 178(1986)416
    H.Satz, Nucl.Phys.A 488(1988)511C

[5] R.Stock, Proc. Quark Matter 1988, to appear in Nucl.Phys.A and G. Young, ibid.

[6] H.Sorge, H.Stöcker, W. Greiner An.Phys. 191(1989)

[7] C.Greiner, P.Koch, H.Stöcker Phys.Rev.Lett. 58(1987)1825 Phys.Rev.D 38(1988)2797
    C.Greiner and B.Mueller, Phys.Bl. 45(1989)152
    E.Farhi and R.L.Jaffe, Phys.Rev.D 30(1984)2379

[8] R. C. Hwa, Oregon Institute of Theoretical Science preprint, OITS 407(1989).

[9] P. Carruthers and M. Duong-Van, Los Alamos preprint, LA-UR-83-2419,
    I. M. Dremin , Mod. Phys. Lett. A 1333(1988).

[10] L. Van Hove, Nucl.Phys.A 447(1985)443c,
    R. Hwa and K. Kajantie, Phys.Rev.D 32(1985)1109.

[11] L. van Hove, Proceedings of the ICPA-QGP'88. Editors: B. Sinha and S. Raha. World Scientific 1988.

[12] B. Andersson et al. Lund Univ. Preprint, LUIP 8808 (1989), accepted for publication in Nucl.Phys. (1989).

[13] R. Albrecht et al. Lund Univ. Preprint LUIP 8903 (1989). To be submitted to Z. Phys. C – Particles and Fields.

[14] W.Weiner, Univ. Marburg preprint
M.Gyulassy, LBL preprint

[15] A.Bialas and R.Peschanski, Nucl.Phys.B 308(1988)857 and Phys.Lett.B 207(1988)59

[16] T.H.Burnett et al.,Phys.Rev.Lett. 57(1986)3249

[17] U.Heinz,Proc. Quark Matter 1988, to appear in Nucl.Phys.A

[18] W.Zajc, Phys.Rev.D 35(1987)3396

[19] A.Bamberger et al., NA35-Collaboration Phys.Lett.B 203(1988)320

[20] S.Pratt, Phys.Rev.D 33(1986)1314
G.F.Bertsch, Proc. Quark Matter 1988, to appear in Nucl.Phys.A

[21] K.S.Lee, M.J.Roades-Brown and U.Heinz, Phys.Rev.C 37(1988)1452, and ibid. p.1463

[22] R. Albrecht et al., WA80-Collaboration, Phys.Lett.B 201(1988)390

[23] L. van Hove, Phys.Lett.B 107(1981)320; Phys.Lett.B 118(1982)138

[24] L.D. McLerran and T. Toimela, Phys.Rev.D 31(1985)545

[25] R.C. Hwa and K. Kajantie, Phys.Rev.D 32(1985)1109

[26] E.V. Shuryak, Phys.Lett.B 78(1978)150
O.V. Zhirov, Yad. Fiz. 30(1978)1098 Sov.J.Nucl.Phys. 30(1979)571

# 2   Large Acceptance Hadron and Photon Detector – Overall Layout

## 2.1   Layout

Fig. 5 shows a schematic top view of the experimental layout. The target is placed at the upstream field fringe of the Vertex magnet now employed in NA35. Its total $\int B dl$, of about 4.5Tm, achieves the necessary dispersion of charged particles in the horizontal plane, with a $p_T$ kick of about 1.2 GeV/c which arranges the charged products into a "butterfly" along the deflection plane, with the highest spatial track density at the center and a slight excess of tracks at the positive side, due to the initial ptoton net charge of 164 in Pb+Pb collisions. At a maximum beam rate of $10^6$ions/s "valid beam" trigger signals are derived from a Quartz Cerenkov counter Q1 placed upstream of the magnet. The subsequent array of tracking and calorimetric detector elements adopts to the butterfly deflection pattern, analyzing charged particles at lab. momenta exceeding about 2 GeV/c (mid-rapidity for pions) and ranging up to about 100 GeV/c, as well as photons in the interval $2.8° < \Theta < 8.6°$ corresponding to the rapidity range $2.6 < y < 3.7$. A set of downstrean trigger calorimeters covers the domain $0 < \Theta < 2.8°$ ($\eta > 3.7$), subdividing into a ring calorimeter (now employed in NA35) for the domain $3.7 < \eta < 5.5$ and a "zero degree energy flux" veto calorimeter for $\eta > 5.5$ that stops the beam.

**Tracking and particle identification**

Charged particle identification and momentum measurement forward of midrapidity is accomplished with a horizontal array of Time Projection Chambers(TPC) and Ring Imaging Cerenkov detectors(RICH). A central large volume TPC, of 4m width, 1.5m height and 4m length, which is tapered in shape to a 5m exit width in order to accommodate optimally the track direction pattern, analyzes particles of $p_{lab} \geq 6$ GeV/c by means of ionization measurement in the relativistic rise, with a $dE/dx$ resolution of about 3.5% and a momen-

14

tum resolution of $\Delta p/p \approx 0.001$. The drift direction is vertical, with a layer of readout electronics on the top surface. This central detector, which passes the beam through a gap and a thin vacuum tube, accepts the essential part of the kaons and protons/antiprotons at $y > 2.9$. Midrapidity pions, however, range down to $p_{lab} \approx 2\,\mathrm{GeV}$ at low $p_T$. They are thus dispersed over a wider horizontal domain by the Vertex field, and their lower $p_T$ fraction cannot be identified by ionization measurement. This is the chief reason for the further, lateral extension of the tracking array, by means of thinner TPCs wich are backed by RICH detector surfaces. To either side, two tracking TPCs of 1.2m thickness provide momentum analysis and tracking into the segmented RICH surfaces. The domain of deflection angles directly adjacent to the acceptance of the central, large TPC, covered by the first pair of lateral thin TPCs, has no RICH backup because the pions in this domain, predominantly of $p_{lab} \approx 4$–$6\,\mathrm{GeV}/c$, can still be identified and separated from the $p$, $K$ fraction by $\mathrm{d}E/\mathrm{d}x$ measurement (even in the 1.2m thick TPC), the latter fraction remaining unresolved which is immaterial because one is dealing with below mid-rapidity $p$, $\bar{p}$ and $K^{\pm}$ here. At further lateral deflection, the RICH surfaces take over in identifying the charged particles. This leads to tightening up the pion identification range down to $y \approx 2.8$, and along with it comes an identification of a fraction of the $p$, $\bar{p}$, $K^-$, $K^+$ yield well below mid-rapidity.

With an increasing height towards the lateral direction (first TPC 2m, second TPC 2.5m) the detectors adapt, in part, to the laterally widening "butterfly" deflection pattern of charged particles. The TPC's consist of a top and bottom subvolume here, and the RICH surfaces are modular, with $1\mathrm{m}^2$ units read out by a CCD camera. Fig. 6 shows the active areas of the TPC – RICH elements as projected onto a plane perpendicular to the beam, 10m downstream of the magnet center. This plane coincides with the front face of the main TPC. The hit pattern obtained with FRITIOF for Pb+Pb, $180\,\mathrm{GeV}/N$ central events is shown superimposed. A total of about 1000 charged particles is accepted per event. The pad granularity of the TPCs is correspondingly high. Pending further experience in the current NA35 tests of a TPC without magnetic field we expect to employ of the order of $10^5$ to $2 \cdot 10^5$ electronic TPC channels in total.

15

## Photon detectors

Two sets of photon high resolution calorimeters are shown in Fig. 5 and 6. A 3200-cell BGO calorimeter of $2m^3$ total active area, positioned 13m downstream of the target, is placed above and below the main TPC. It subtends the interval $5.8° < \Theta < 8.6°$, $2.6 < \eta < 3.0$ and is placed (Fig. 6) in the azimuthal domain that is essentially free of charged particles due to the sweeping of the Vertex magnet. For the sake of complete charged particle hit discrimination/rejection the two BGO surfaces are covered by a Charged Particle Veto (CPV) detector. The CPV also detects the charged products of $\Lambda$ and $K_0$ decaying outside the Vertex field (and, thus, are not swept out of the BGO acceptance). As the granularity of the present WA80 streamer tube arrays ($10 \times 25mm^2$) is not sufficient in combination with the high spatial shower resolution of the BGO array ($25 \times 25mm^2$ cell size) we intend to employ a gated multi-step parallel plate avalanche chamber, with Argon-Methane gas and TEA vapour filling. This will permit visual imaging of individual avalanches (recording by CCD cameras).

A second set of photon calorimeter surfaces is placed about 31m downstream of the target, again above and below the beam but subtending an adjacent interval, $2.8° < \Theta < 4.8°$ and $3.2 < \eta < 3.7$. The material employed here is the $38 \times 38mm^2$ Pb-glass (SF5) structures now used in WA80 and GAMS. This granularity is sufficient at the large distance. The up/down detector surfaces are again protected by appropriate Charged Particle Veto arrays.

## Trigger calorimeters

The "Ring" calorimeter of NA35, placed now at 32.5m distance from the target, consists of an EM and a hadronic portion and has a concentric-ring cell structure arranged in 12 constant steps of pseudorapidity. Its inner hole, of 56 cm diameter, passes all particles of $\eta > 5.5$ through to the "zero-degree-Veto" calorimeter which also stops the beam. A new construction is required here, to accomodate a beam flux of $10^6$ ions/s, the wider dynamical

16

range required with Pb projectiles (36TeV), and the extended illuminated surface as defined by the bore of the Ring calorimeter.

If one wants to go beyond the usual veto on energy flux at $\Theta < 0.3°$ for centrality selection of the events one could likewise pull additional ring sectors of the Ring calorimeter into the veto. The Ring calorimeter can also serve to establish an interaction trigger by requiring a nonzero $E_T$, in addition to the "less than the beam" signal in the zero degree calorimeter.

## 2.2 Beam rate, interaction rate, data rate

The two most stringent factors limiting the interaction rate capability stem from the maximum drift time in the TPC, and from possible event-rate related space charge accumulation in the TPC. Both problems are now estimated to be of little relevance below an instantaneous interaction rate of about $2 \cdot 10^3$/s. A 0.2% interaction thickness target would yield this rate with a $10^6$ ions/s instantaneous beam intensity. Triggering on the 5% fraction of "most central" events (by zero degree energy veto) and assuming a 50% deadtime then leads to a central trigger rate of about 50/s. This coincides with the readout speed of the next generation of 1M-pixel CCD cameras which will be employed in the RICHes and in the Charge Particle Veto arrays of the photon detectors. These devices could thus operate with 50Hz data rate, provided an online data compression before data storage. The large TPC, on the other hand, is (intrinsically much faster but) data rate limited to about 2–10Hz because of its high output size per event.

Thus all devices can run concurrently at 2KHz interaction rate and $10^6$/s beam rate. The photon detectors would gather 5–20 times higher statistics by themselves, every fifth event being backed up by the full tracking/hadron identification complex, if this operates at 10Hz.

17

## 2.3 Extension by a second Magnet

Of our intended major physics goals two probes, in particular, would substantially benefit from placing the main TPC into a magnetic field: we could then analyze neutral strange particle yields ($K_0$, $\Lambda$, $\overline{\Lambda}$), thus completing our measurement of the quark flavour composition of the final state. Also, HBT correlation analysis would improve drastically at $\Delta p \to 0$ by higher momentum resolution. Fig. 5 thus schematically depicts the contours of a large second dipole magnet housing the main TPC. We consider this as an extension option. The BGO arrays would then move to a different position, without major rearrangements occuring with respect to position and acceptance of the other components.

# 3 Détecteurs

## 3.1 The Time Projection Chamber

The high charged-particle multiplicity in a high-energy Pb-Pb collision makes it essential to use continuous tracking in three dimensions. The Time Projection Chamber (TPC) is the only electronic detector with sufficient capabilities[1]. In addition to excellent tracking the TPC provides particle identification by ionization loss measurement in the relativistic rise regime. It is a very low mass detector avoiding conversion of the abundant photons.

The application of a TPC for tracking and $dE/dx$ measurements in $^{32}$S collisions has been described in detail in the NA-35 TPC Proposal to the SPSC[2], where the construction and performance of a TPC which can be regarded as a prototype for the present experiment is described. Here we outline only the main features, emphasizing that actual performance at track densities equal to those expected in the present configuration for Pb-Pb collisions will be tested in the 1990 $^{32}$S running, and detailed decisions on how to proceed can be made after those results are available.

### 3.1.1 Technique adopted

The TPC technology we adopt is firmly based in experience with the classic PEP-4 TPC and on the extensive developments made at CERN, especially with ALEPH. The concept of pad-only readout for tracking and $dE/dx$ was developed for the study of high-multiplicity heavy ion collisions at the Bevalac[3] and is being implemented there in a 24000 channel TPC (the HISS TPC) for operation in 1991[4]. However, the adaption ends where new electronics need to be developped (see sect. 4).

### 3.1.2 Tracking and momentum measurement

The tracking capabilities of the pad-readout TPC are at least as good as those of conventional TPCs since a larger number of pad rows can be utilized. The pad-readout mode

eliminates the problem of multiple hits on individual wires, providing very good two track separation capability. The momentum resolution in the present experiment differs for the various TPCs but is in the region of $\Delta p/p = 0.001p$. The two-track separation is of the order of $1cm$ and has been discussed in detail in ref.[2].

### 3.1.3 Particle identification

The capability for particle identification by ionization is demonstrated in Figure 7, which shows how the truncated mean of many ionization samples depends on particle momentum and mass[5]. The resolution in $I/I_0$ depends primarily on the thickness of the TPC and secondarily on the numbers of samples. For the two thicknesses of TPCs which we propose the resolution is expected to be $\sigma(I/I_0) = 0.033 \, I/I_0$ for the 4m TPC(100 4cm samples) and $\sigma(I/I_0) = 0.06 \, I/I_0$ for the 1.2m TPC(30 4cm samples). The latter is the same thickness as the one being tested in NA-35 during the 1990 running period.

### 3.1.4 Experimental layout

The configuration of Figure 5 is based on locating the target in a "vertex" magnet. The magnet provides spatial separation of particles of different momentum, allowing momentum measurements by tracking detectors and TPCs. It also produces an essential reduction in track density in the forward direction. The spatial separation of particles of different momentum also allows the use of appropriate detectors in different momentum regimes, simplifying the particle identification problem. The primary work of particle identification is done in the forward detector, which contains most of the protons and kaons. The 4m thickness of the TPC permits $\pi$, $K$, $p$ separation, which we have assumed to be sufficient in the ranges shown in Table 1.

The performance of the 4m-TPC is illustrated in Figure 8, where the particle ratios are taken from FRITIOF. For particles outside of this domain the ionization for $K$ and $p$ is so similar that there is no possibility of separation by ionization. Thus it is possible

20

Table 1: Particle identification criteria adopted for exploratory acceptance studies.

|  | 4m TPC | 1.2m TPC | RICH |
|---|---|---|---|
| $\pi$ | 2–70 GeV/c | 3–20 GeV/c | up to 3 GeV/c |
| $K$ | 6–70 GeV/c | none | up to 3 GeV/c |
| $p$ | 6–70 GeV/c | none | up to 5 GeV/c |

to relax the thickness of the TPC and to concentrate on pion identification, which is achieved between 3–20 GeV/c with a 1.2m thick detector. The performance for 3 GeV/c and 5 GeV/c particles is illustrated in Figure 9. In the last angular range the TPC is used only for tracking, particle identification being provided by RICH detectors. (There is an intermediate regime when both TPC and RICH detectors are used to cover the entire range of energies of the incident pions). The distances of the detectors to the target have been chosen on the basis of FRITIOF calculations of central Pb+Pb collisions so that losses due to multiple hits stay below 20%. In fact losses are in the region of 5–10% everywhere, except in the extreme forward direction where they approach 20%. These estimates are approximate and will be refined after experimental information has been obtained on the proton distribution. The layout presented is obviously schematic and does not yet address important problems of construction, avoiding acceptance gaps between the detectors, accommodating the beam pipe etc. One point is important, however, in our schematic design. That is that we desire to use as large detector volumes as possible, to avoid acceptance gaps and to avoid the introduction of unnecessary material into the intense flux of photons and neutrons associated with each event. These, as well as the charged particles, could cause substantial backgrounds in more finely segmented detector arrays.

21

### 3.1.5 Acceptance

The acceptance achieved for this conceptual design is shown in Figure 10 for $\pi^-$, $K^-$, $p$. More than half the produced pions and antiprotons are detected and identified and over one third of the kaons. The total number of charged particles identified is about 1000 per central event. This is achieved with a total of 100.000 readout channels of electronics (80.000 for the 4m TPCs, 20.000 for the 1.2m TPC and 4000 for the tracking chambers).

Figure 11 shows the coverage in $y-p_T$ space achieved for identified pions (from FRITIOF) together with the corresponding distributions for all produced pions.

## 3.2 Large volume TPC inside a magnetic field

In an extension of the layout discussed thus far, we are currently investigating the option to place the central, large volume TPC, of about $4 \times 4 \times 1.5 m^3$ size, inside a magnetic field. This configuration offers the following advantages:

(a) Neutral strange particle decays, chiefly $\Lambda$ and $\overline{\Lambda}$, could be analyzed in the magnetic field. In the rapidity interval $4 < y < 5$ the mean Lorentzfactor $\gamma$ of $\Lambda$, $\overline{\Lambda}$ is about 50, securing a reasonable fiducial volume in which 3% of the decays occur. Scaling up from the $\langle \Lambda \rangle$ observed in central S+S collisions, we expect a total mean $\Lambda(\overline{\Lambda})$ multiplicity of 60(6) per Pb+Pb central event even if no further strangeness enhancement occurs. A subensemble of $10^5$ TPC events then offers $3 \cdot 10^4 (3 \cdot 10^3)$ $V^0$ decays of $\Lambda(\overline{\Lambda})$. Measurement of these cross sections would complement the $K^+$, $K^-$ yield information, enabling us to obtain a reliable strange- to nonstrange quark ratio within subensembles of the total TPC event pool which are selected according to various criteria (high $p_T$, large HBT source radius etc.) imposed at the event by event level.

22

(b) The momentum resolution is substantially improved by the additional momentum dispersion in the (second) magnetic field over a 4m track length. This extends the range in $y$ and $p_T$ of precision $2\pi$, $2K$ correlation analysis.

(c) At a mean distance of 12m from the target of the central TPC, decays in flight of $\Lambda$ and $K$ outside the field of the VERTEX magnet lead to a significant fraction of tracks in the TPC that do not stem from the primary vertex. Magnetic analysis in the second $B$-field enables a precise discrimination of tracks from such secondary decays.

A suitable magnet, of reasonable field homogenity over a $4 \times 4 \times 2\text{m}^3$ volume at a field level upward of 1T does not exist at CERN. A preliminary design study, of a structure similar to the CERN VERTEX magnet but employing non-superconducting Al coils of L3-type leads to a 1200 t-magnet of only 3 MW power consumption. We have entered into negotiation with our collaboration partners from Bombay/Calcutta and Zagreb toward providing such a magnet, under the auspices of the emerging CERN collaboration agreements with India and Yugoslavia.

Fig. 5 shows a sketch of such a magnet within the overall layout. A slight re-arragement of the various components may be necessary due to the expected fringe fields and outer dimensions of the second magnet leading, however, to no major change in the acceptances of the external components.

## 3.3 The RICH Detector

The chief purpose of the RICH arrays considered here is to tighten up our hadron identification range, down to midrapidity and low $p_T$ where the TPC does not identify pions and kaons.

Detailed Monte Carlo calculations have shown that even in the high multiplicity central collisions between $^{208}\text{Pb}+\text{Pb}$ one should be able to separate $\pi$'s from $K$'s for $1 < p_{lab} < 3.5$

and $K$'s from $p$'s for $1 < p_{lab} < 5$ with good efficiency, utilizing a liquid freon Ring Imaging Čerenkov Counter (RICH). For the charged particle identification the momenta of the charged particles must be measured. This will be done by the TPCs described earlier. Since they are in the field free region the track trajectories will be straight lines, which simplifies the track reconstruction.

In the scheme used in the RICH counter, shown in Fig. 12, the charged particle first traverses the multistep avalanche counter, the synthetic quartz window and then the liquid freon radiator (FC-72). The emitted Čerenkov photons are focused back into the detector by an array of spherical mirrors specially constructed to have a high reflectivity in the UV. The UV photons convert in the TMEA of the first gap of the multistep avalanche counter. The number of produced electrons is largely increased in the *gated* second field gap of the detector. The electron cloud drifts into the $3^{\text{d}}$ multiplication gap, where the photons from the gas amplification are detected by an image intensified CCD camera for every $m^2$ of detector. In order to get the required position resolution in the detection of the UV photons, the cameras will have $1K \times 1K$ pixels. There will be a total of 16 cameras for the four RICH modules.

By following the trajectory of the charged particles from the tracking chambers to the RICH, and knowing their momenta, the detected Čerenkov pattern is compared to the one expected for $\pi$, $K$ and protons. The best fit gives the particle identification.

The RICH detector has been segmented, into two parts at each side for the positive and negative particles, in order to optimize the acceptance, keeping the size and double hits to a minimum. The dimensions and positions used in the acceptance calculations illustrated below are:


- RICH-1 size 1.5m horizontally × 2.4m vertically at 12m from the target covering the interval $12° < \Theta < 20°$


- RICH-2 size 2m×2m, at 9m from the target covering the interval $21° < \Theta < 34°$

24

This geometry accepts on the positive side 150 pions, 7 kaons and 28 protons in central Pb+Pb collisions (Fritiof simulation). The accepted pions fall in the $2.1 < y < 4.1$ region, the kaons between $2 < y < 3$ and the protons between $1.2 < y < 2.4$. The acceptance plots are shown in Figures 13,14. The detector positions implied by the layout in Fig. 5 are slightly different, shifting the RICH detectors further outward in order to optimize the coincidence of *accepted* and *identifyable* particles. This results in the compounded TPC-RICH identification ranges as given in Fig. 10 and 11.

A 20cm×20cm prototype RICH detector with this geometry, constructed by Giomataris et.al.[6] has been tested in the beam with a liquid freon radiator[7]. A larger 50cm×50cm detector with multiple mirrors is being tested by NA35, and a larger 1m×1m will be developed by NA35 to be used in the next $^{32}$S beamtime.

## 3.4   The BGO Detector

The effort required to obtain cross sections for direct photon production has three main steps, the second of which yields also the $\pi^0$ and $\eta$ cross sections. These steps are:

1. Measure the invariant cross section for inclusive single photon production over the $y$ and $p_T$ range of interest

2. Determine the invariant cross section for $\pi^0$ and $\eta$ mesons over the same range

3. Correct the inclusive photon cross section by subtracting the cross sections for photons emitted in $\pi^0$ and $\eta$ decay and from radiative decays of, e.g. high lying resonance states and hyperon decays.

This last step requires a Monte Carlo using the measured cross sections of step 2 as one of its input. One way to present the results is as a ratio of $\gamma$ to $\pi^0$ cross sections, thus cancelling systematic uncertainties due to target thickness, beam intensity and deadtime.

The design study for a photon detector thus becomes in large part an exercise in making a detector which can measure $\pi^0$ and $\eta$ cross sections in the presence of combinatorial

("false") pairs of photons. This problem is exacerbated in heavy ion collisions, relative to p-p collisions, due to the much higher multiplicity of produced particles; the peak/background ratio in a two-photon invariant mass spectrum varies as $1/M_\gamma$, where $M_\gamma$ is the multiplicity of final state photons, which is dominated by $\pi^0$ and $\eta$ decay.

We propose to identify photons by fitting their transverse shower shape in a highly segmented electromagnetic calorimeter. We then need to choose a detector geometry and a number of pixels for this detector and a detector material. Hadron and charged particle rejection will be improved by the addition of a pixel-readout multiplicity detector just in front of the electromagnetic calorimeter. This technique is similar to that used in WA80.

The number of pixels needed is determined by the multiplicity of particles (charged particles, neutral hadrons and photons) falling within the pseudorapidity and azimuth range to be covered, times $1/f$ where $f = 3\%$ is a pixel-filling factor found to give a reasonable separation of neighbouring showers in the SAPHIR lead-glass array of WA80. The number of pixels required to cover all azimuth for a given pseudorapidity interval can then be estimated using the prediction for the particle multiplicitiy of the the string model FRITIOF. The required detector distance at a given pseudorapidity is then determined by the pixel size for a given detector type, which is closely related to the Moliere radius for that detector material. A smaller Moliere radius allows a smaller target distance, with a linear relationship between the two. Results for BGO ($2.5 \times 2.5$cm$^2$ pixels) and SF5 lead-glass ($3.8 \times 3.8$cm$^2$ pixels) are shown in Figure 5 as a function of detector angle (or pseudorapidity). The distances for SF5 are 52% larger.

The next issue to be discussed, and the one which drives the choice of detector technology the most strongly, is that of identifying the $\pi^0$ and $\eta$ mesons. Since these particles decay quickly and are detected by observing neutral decay products, no vertex location is possible, and these particles must be identified from two-photon invariant mass plots. The peak to background ratio in such a plot, at the location of the $\pi^0$ or $\eta$ relates inversely with the photon multiplicity and linearly with the invariant mass resolution of the detector. As the photon multiplicity is set by the choice of reactions to be studied, our only method of

improving this peak to background ratio lies in improving our invariant mass resolution.

From present experience with detecting $\pi^0$s in the SAPHIR array in collisions at $E/A = 200\,\mathrm{GeV}$ $^{16}$O+Au and $^{32}$S+Al, we know that a peak to background ratio of $\simeq 1:1$ can be achieved, summed over all $p_T > 1\,\mathrm{GeV/c}$. This ratio improves with increasing $p_T$ of the photon pair. Because the photon multiplicity is about six times larger in Pb+Pb than in O+Au collisions for the same bombarding energy, we must seek a technique offering an invariant mass resolution that is correspondingly about six times better than the $\sigma_m/m \simeq 6\%$ achieved with SAPHIR, in order to obtain similar values for the peak to background ratio.

The invariant mass resolution of the detector chosen depends on both its intrinsic energy resolution and on the ratio of its position resolution to distance from the target. The calculated invariant mass resolution for $\pi^0$ and $\eta$, for detectors made from BGO, type SF6 lead glass and type SF5 lead glass, are shown in Figures 16a and 16b. The figure shows the percent invariant mass resolution, $\sigma_m/m$, as a function of $p_T$ for four choices of rapidity. The calculation allows for all decay orientations in the parent rest frame. An asymmetry cut of $\alpha < 0.6$, where $\alpha = |E_{\gamma_1} - E_{\gamma_2}|/(E_{\gamma_1} + E_{\gamma_2})$ is applied. This does not strongly affect the results, as energy thresholds of $E_\gamma = 50\,\mathrm{MeV}$ for BGO and $E_\gamma = 400\,\mathrm{MeV}$ for the lead glasses are applied first.

The energy resolutions assumed were:

| | | |
|---|---|---|
| BGO | $\frac{\Delta E}{E} = 1.5\%/\sqrt{E}$ for $E_\gamma < 9\,\mathrm{GeV}$ | |
| | $\frac{\Delta E}{E} = 0.5\%$ constant for $E_\gamma > 9\,\mathrm{GeV}$ | (L3 experience) |
| SF6 | $\frac{\Delta E}{E} = 5.0\%/\sqrt{E}$ | (OPAL/KEK experience) |
| SF5 | $\frac{\Delta E}{E} = 6.0\%/\sqrt{E} + 0.4\%$ | (WA80 experience) |

The position resolution assumed were:

| | |
|---|---|
| BGO | $\Delta x = 1$mm above $E_\gamma = 10\,\text{GeV}$, |
| | (linear variation below with a value 3mm at 1 GeV) |
| SF6 | $\Delta x = 2$mm |
| SF5 | $\Delta x = 3$mm |

The detectors were placed at 20 meters for $2° < \Theta < 12°$ and 10 meters for $12° < \Theta < 45°$; no acceptance was assumed outside this theta range. Actually, based on Moliere radii, larger distances would be used for SF6 and much larger for SF5 to satisfy the pixel filling criterion in an actual experiment; the distances were kept fixed for the calculation to point out the resulting difference in mass resolution.

The rise in $\sigma_m/m$ at low $p_T$ is due to the energy resolution term and that at high $p_T$ is due to the position resolution term, as is well known. For $y < y_{cm}$ ($y_{cm} = 2.92$ for 160 GeV/Nucl.) the energy resolution term dominates over most of the $p_T$ range. The position resolution is more important for $y > y_{cm}$, except for the $p_T$ range below $\sim 1\text{--}1.5\,\text{GeV/c}$. However, for the purposes of a heavy ion experiment, this $p_T$ region is of great importance, as discussed in section 1.

This improvement in resolution with BGO in contrast to the SF5 used presently in WA80 can be seen in the following figures. We have performed calculations of the invariant mass spectrum, including both combinatorial and true pairs of photons, to be expected in detectors made of BGO and SF5. We used the FRITIOF code to generate the minimum bias events we discuss first. The size of the BGO and SF5 arrays were chosen assuming a constant financial investment of \$5M for each. Their distances were chosen according to Figure 15 above. The BGO was located between polar angles of $4.4° < \Theta < 5.7°$ (one quarter unit of pseudorapidity) and spanning two ranges in azimuth $26° < \phi < 106°$ and $176° < \phi < 217°$. (These were chosen as a tradeoff between $\pi^0$ and $\eta$ acceptance at $p_T < 1\,\text{GeV}$.) The SF5 was located just forward of the BGO, at $3.5° < \Theta < 4.4°$ and spanning $0° < \phi < 106°$ as well as $176° < \phi < 282°$ (the lower cost of the SF5 is reflected

28

in its greater coverage). The actual positions given in the layout of Fig. 5 are slightly different but not such as to change the results.

The results for the BGO are shown in Figure 17 for 12000 minimum bias Pb+Pb events. It shows the invariant mass spectrum in the region around the $\pi^0$ mass, for both true and combinatorial pairs. It can be seen that a clean $\pi^0$ peak is obtained for $p_T > 0.5\,\text{GeV}/c$, with less satisfactory behavior below. The companion results for the SF5 detector are shown in Figure 18. It can be seen that, even though the number of counts is much larger, the accuracy with which the $\pi^0$ cross section may be extracted will be much worse, due to the significantly poorer mass resolution.

In order to study the situation for the central collision events which are of primary interest to us, we constructed a special event generator for central events. (It is quite consumptive in computer time to run FRITIOF for this purpose for Pb+Pb). The pseudo-rapidity, $p_T$ and multiplicity distributions for $\pi^0$ and $\eta$s as given by FRITIOF for a small sample of central events are fairly well reproduced. We then generated 25000 central events and again computed the invariant mass spectra. Those for BGO are shown in Figure 19a,b while those for the SF5 are shown in Figure 20a,b. The statistics are of course more than a factor of two better due to the much higher multiplicity of produced particles in the central events. The markedly superior behavior of the BGO is obvious. We remark that this large number of central events represents about one hour's worth of running with a central event trigger at our anticipated data-recording rate of 50 events/second for the photon part of the experiment. We also remark that for $p_T > 2\,\text{GeV}$ it might be possible to reconstruct individual $\pi^0$s even on an event by event basis in the very high multiplicity enviroment of Pb+Pb collisions due to the better than 10 : 1 peak to background ratio in the invariant mass spectrum at these larger $p_T$ values.

There are several candidate materials for an electromagnetic calorimeter which can reach the 1% level for the statistical term in energy resolution. These include BGO, NaI(Tl), CsI(Tl), CsI, BaF$_2$ and some scintillating glasses. We reject the last from further consideration due to the large constant terms reported for their energy resolution and

because of their large radiation lengths ($X_0$ = 4.35cm for SCGI-C glass) and Moliere radii. We estimate the cost per pixel using a pixel volume defined as one Moliere radius squared (transversed area) by 22 radiation lengths deep. This eliminates BaF$_2$ due to its high cost (it also is complicated to read-out due to its short wavelength emission). This leaves the first four inorganic cristals listed which have similar cost per pixel. We would not like to employ NaI(Tl) due to its need for a can to avoid problems with its being hygroscopic. We then prefer BGO to CsI(Tl) or CsI because of better hardness, shorter scintillation decay time, radiation resistance, smaller size, self-curing properties after radiation damage and less after-glow. CsI(Tl) gives out about three times as much light per square Moliere radius, but we feel the advantages given above for BGO outweigh this. CsI would require in addition a special photodiode or photomultiplier tube to detect its short wavelength light output, so we did not consider it further, as we have no obvious need for its great speed.

### 3.4.1 Experimental Layout of the photon detector

The BGO photon calorimeter will identify $\pi^0$ and $\eta$ mesons around the midrapitity region of Pb+Pb collisions. Because of the extremely steep angular distribution of particles in the very forward region $y \geq 3$, we plan to cover the backward hemisphere starting at midrapidity, $2.58 \leq y \leq 2.98$. This will allow optimum use of the detector in terms of obtaining a fairly uniform hit propability of modules over the solid angle of the detector. Nonetheless, the distance of the detector to the position of the target is dictated by the particle density at $\eta = 2.98$ ($\Theta = 5.8°$). Based on our experience with WA80 Saphir detector we learned that a *primary* hit propability of 3% in each individual module can be handled. With the planned module size of 2.5 × 2.5cm$^2$ for BGO modules this translates – according to FRITIOF simulations of central Pb+Pb events – to a distance of 12.3 m if only neutral particles ($\gamma$, $n$, ...) are considered, and to $d = 17.3m$ if both neutral + charged particles are entering the detectors. This factor of roughly 2 in particle density (i.e. $\sqrt{2}$ in distance)

30

in these two cases demonstrates already the benefit from a strong vertex magnet positioned at the target if the photon detectors are operated in the charged-particle-depleted region. Since we intend to place the BGO detector in a two-arm geometry above and below the TPC, i.e. in the region where there are only very few charged particles, we are able to locate the detector a distance of 13m from the target. Extensive MC-simulations were carried out to obtain optimum acceptance for $\pi^0$ and $\eta$'s. This has been done both by pure kinematical and geometrical acceptance calculations, as well as by making use of FRITIOF simulated events. As a result it turned out that a minimum solid angle corresponding to a detector surface of 2m$^2$ is required, and that this area is most effectively used in a two-arm geometry with one arm having on opening angle of $\Delta\phi = 80°$ and the second of $\Delta\phi = 40°$. The bigger arm thus enables to reconstruct $\pi^0$ down to $p_T \simeq 300\,\text{MeV/c}$, while the second arm – beside $\pi^0$ reconstruction – allows low $p_T$, $\eta$ reconstruction when used in conjuction with the other arm. A sketch of the geometrical layout is shown in Figure 21. Since the outermost modules of such a high-granularity calorimeter cannot be included in the shower reconstruction algorithms, because of asymmetric energy leakage out of the detector, we intend to build a frame of two rows of modules around the central BGO part of the detector consisting of a less expensive detection material. The material which fulfills closely the requirements of having a similar radiation length and a similar Moliere radius to that of BGO is SF6 lead glass.

### 3.4.2  Charged particle rejection for photon measurements

In order to reject the background of charged particles when measuring photons an effective veto detector is needed. It is of utmost importance that this detector has high efficiency and good spatial resolution. It is furthermore necessary that this detector be capable of operating at the same rate as the photon detector system. The high efficiency is needed to suppress background from charged particles. This is extremely important when reconstructing the $\pi^0$ and $\eta$. A good spatial resolution is needed to determine the hit position of

a charged particle. It is furthermore of great advantage if the resolution is comparable to that of the photon detector resolution since this will improve the shower reconstruction of charged particles. This is particularly important in a high-multiplicity environment such as that produced in Pb+Pb collisions at SPS energies. In these collisions the probability of having a charged particle very close to a neutral one is large. Therefore, the accurate determination of the location of charged particles will greatly improve the efficiency of the photon detector. The proposed multiplicity detector will have a resolution of the order of 2 mm.

The detector will be a gated multi-step parallel plate avalanche chamber (PPAC) with a filling gas of Argon-methane containing the vapour of triethylamine (TEA), permitting the visual imaging of the avalanche. This technique was pioneered by Charpak and collaborators. Chambers reported in the literature are small, typically $10 \times 10 \text{cm}^2$. For our application it is important to find a design that allows the active area of the detector to be one square meter.

The position resolution is expected to be about 2mm. Comparing with the smallest pad size ($10 \times 25 \text{mm}^2$) in the present WA80 streamer tube multiplicity detectors, the position resolution will increase by a factor of 5–10 and the multi-hit probability will be reduced by this factor squared, i.e. around a factor of 50. Light yields of greater than $10^6$ photons per avalanche have been reported, permitting full detection efficiency with conventional optics.

TEA radiates only in the UV, and a wavelength shifter will be placed close to the light-producing anode to shift the radiation to the visible region. The avalanche can then be imaged by a CCD camera equipped with an image intensifier. The data rate from the camera will be very high, and it will be necessary to perform real-time data reduction. A triggerable 100Hz CCD camera system, suitable for this application, is currently under development at the company EEV in England.

A small test chamber ist presently being operated, and further tests will soon be made on a full-size $50 \times 50 \text{cm}^2$ chamber. In the calibration beam period in Noc.-Dec 1989 the detectors will be tested in real beam conditions.

## 3.5 Triggers and Calorimeters

The zero degree trigger calorimeter, again based on past experience (see sect. 2.1), will be located behind a larger calorimeter, which will effectively act as an active collimator. In order to account for the dispersion introduced by the Vertex Magnet, which causes a separation between neutron fragmentation products, the primary beam and proton fragmentation products, the aperture in this calorimeter will be rectangular. Located at about 35 meters, the horizontal dimension of the slit is expected to be the order of 25-35cm. The existing NA35 Ring Calorimeter, with appropriate modifications, may be suitable for this purpose.

A new Zero-Degree Calorimeter will be constructed, since neither of the two existing devices is capable of providing full containment given the the proposed layout. The new ZDC will be consistent with the size of the aperture in the collimating calorimeter, and will have to be capable of handling the anticipated beam rates of the 34TeV Pb projectiles. One possible design consists of a lead-plastic scintillator sampling calorimeter (lead/plastic ratio of 4 : 1 to assure compensation) of octagonal cross section (about 90cm side to side) with a length of about 2m. The broad dynamic range would be obtained via a dual-ADC readout. Fast wavelength shifter material would be used to assure high-rate capability.

In addition to the ZDC trigger, two other trigger systems are contemplated. One is a general interaction trigger whose role will be similar to the current multiplicity trigger of WA80; the other is a cluster-type second-level trigger associated with the BGO detectors.

33

# References

[1] F. Sauli, Z.Phys C38, 339(1988)

[2] CERN-SPSC-89-17, SPSC/M-440, March 6, 1989

[3] H.G. Pugh et al., LBL-22314, Dec. 1986

[4] H. Wieman and H.G. Ritter, LBL, private communication
    and internal reports

[5] I. Lehraus et al., IEEE Trans, Nuc. Sci, NS 30, 50(1983)

[6] Y. Giomataris et. al. preprint CERN-EP/88-96 (1988).

[7] G. Vasileiadis et. al. presented at the 4th Pisa Meeting for Advanced Detectors, May
    21-25, 1989.

# 4 Readout and data acquisition

## 4.1 TPC front-end electronics

The TPC will have 100 K–200 K of channels and therefore needs an unprecedented degree of integration.

Each pad signal is amplified in a charge sensitive amplifier/shaping amplifier which has a peaking time of about 150 nsec, a width of 150–180 nsec (FWHM), a dynamical range of 1000:1, and a noise of 300–500 NEC. The signal is stored in an analog pipeline storage, with a writing speed of 10 MHz, a reading speed 2 MHz, and a depth of 512 capacitors. The signal is digitized by an 8-bit, 1–2 MHz ADC and written into a memory. In the anticipated concept the event is transferred within about 1 msec from the analog-storage into the memory.

The electronics (Fig.1) is mounted in the back of the pad plane. After zero suppression, setting-up of a hitlist and may be clusterfinding and tracking, the data are sent out for storage or further online processing.

We are encouraged to develop this new kind of highly integrated electronics by the enormous progress towards that direction recently achieved at different places. In a joint venture between CERN, Rutherford Lab and the University of Lausanne a highly integrated charge sensitive amplifier (CERN), analog pipeline memory (Rutherford) and a Pipeline-ADC (Lausanne) are under development. In addition, a similar concept is developed at LBL for the HISS-TPC, where a 16 fold 256 channel switched capacitor array is presently being tested.

We intend to test all those chips immediately when they are made available to us either in the TPC-90 (ALEPH), in the NA35 TPC or at LBL in order to evaluate their performance. Since the major components are already existing or being finished soon, it will be our main task to integrate those different components into a system and to increase the compactness. For the time being an integration of 32 channels/chip seems to

be feasible. but we believe that a higher degree of integration is desirable and might be possible in the future.

We aim at a price of 20.- to 30.- SFr/channel which is about a quarter of the price that ALEPH paid. We expect to reach this goal by the higher degree of integration. In the development of the system we envisage a close collaboration between CERN and our participating institutions, in particular MPI Muenchen, LBL Berkeley and GSI Darmstadt.

## 4.2  TPC Data aquisition

### 4.2.1  General considerations

**Estimate of data flow**

In the following an estimate of the data flow expected from the various detectors is made.

**Large TPC with d$E$/d$x$:**  The total amount of data from a large TPC with 100.000 channels would be 50 MB/event (512 time samples). For a single track crossing 1 padrow there will be about 5 time samples above threshold for 5 neighbouring pads. These numbers are average, i.e. for a particle with the most probable d$E$/d$x$ in the center of the chamber. After zero suppression and some filtering (at least two consecutive digitizings for 2 adjacent pads are above threshold) this is reduced to: $5 \times (5 + 2 + 2) + 1 = 46$ bytes:

$$5( \text{ pads } ) \quad \times \quad [5( \text{ time buckets } ) + 2( \# \text{ of 1. time bucket and length } )$$
$$+ \quad 2( \text{ pad } \# )] + 1( \text{ padrow } \# )$$

For 100 padrows this is 4600 bytes/track. According to FRITIOF there will be about 1200 charged particles in the phase space region that is attempted to be covered by TPCs, resulting in 5.5 MB/event. This can be regarded as the net data rate. It is important to point out that this estimate is independent of the actual configuration of the TPCs. Only the total number of tracks enters in the calculation.

**Tracking TPC in front of RICH:** According to FRITIOF there will be about 200 charged particles on either side of the beam in the acceptance of the RICH and tracking TPC. The overall design of this TPC will be very similar to the NA35 downstream TPC. The tracking length will be 120cm, subdivided into 6 evenly spaced padrows, each 4cm large. For 6 padrows this is 276 bytes/track. With 2 × 200 tracks the total amount of information from the tracking TPC is 110 kB/event.

**RICH detectors:** Each particle crossing the radiator will create about 20 photoelectrons, which will be amplified in a two stage avalanche chamber. The light produced in the last stage will be detected with CCD cameras equipped with image intensifiers. Each photoelectron will produce a cluster of 10 pixels in a 1000 × 1000 CCD. There will be 3 × (3 + 4) = 21 bytes/photoelectron:

3( pixels $x$ direction ) × [3( pixels $y$ direction)

+ 4( column, row and subdetector identification and length of string)]

For 2 × 200 tracks total there will be 2 × 200 × 20 × 21 = 186 kbytes/event. This is about the same order of magnitude as the tracking TPC in front of it. However, one has to recall that the RICH arrays operate with 16 CCD cameras, 1 Mpix. each, such that the raw output is 16 Mbytes/event. Thus, the RICH requires massive on-line data compression.

## Data reduction

From the above estimates it seems prohibitive to consider writing the original tracking and RICH information directly to tape. Even with very optimistic assumptions about the availability, speed and price of storage media rates of 40 MBytes/s (averaged over spill) are impossible to store for running periods of 2 weeks. Therefore it is crucial to reduce the primary data flow by about one order of magnitude, or more.

Due to the way the data are generated in the TPC a data reduction in two steps is considered here, each reducing the amount of data by one order of magnitude. The first step is necessary as stated above, the second optional.

**Hit reconstruction:** A considerable reduction in data flow is possible if one considers to calculate online the centroid of the crossing points for each particle with a padrow (called "hits" here). The result is the $y$-coordinate (pad direction) and the $z$-coordinate (time direction) and the integral of the distribution ($dE$). The amount of data from this procedure is: $2 + 2 + 2 + 1 = 7$ bytes/hit:

$$2(x \text{ coordinate }) + 2(y \text{ coordinate }) + 2 \left( \frac{dE}{dx} \right) + 1( \text{ padrow } \#)$$

The total data volume is then $7 \times 100 = 700$ bytes/track and $700 \times 1200 = 840000$ bytes/event or 840 kB/event. For the $x$ and $y$ coordinate the information could be packed into 3 bytes. This estimate is therefore an upper limit.

**Track reconstruction:** The largest reduction in data rate is achieved by online track reconstruction. This is a rather complicated task and requires complex reconstruction algorithms running online on very fast processors. At this point it is regarded as rather risky to throw away the original tracking information ($x$, $y$, $dE$ from each padrow) at this early stage. It seems to be feasible to do online tracking for a TPC outside the magnetic field due to the simpler algorithms involved for straight tracks. A TPC inside a magnet has to deal with curved tracks and in addition with the problem of corrections due to unavoidable inhomogeneities of the magnetic field.

One very important aspect of a data acquisition scheme incorporating online hit reconstruction is the possibility to fully reconstruct a subsample of events online for monitoring and control purposes (this would correspond to the "express line" in UA1 experiment.) This requires extremely powerfull processors and the proper architecture, anyhow. The amount

of information to be stored after a successfull track reconstruction can be estimated to be 12 bytes/track or 14.400 bytes/event:

$$5(x, y, z \text{ at beginning of track }) + 5(x, y, z \text{ at end of track }) + 2\frac{dE}{dx}$$

## 4.2.2 TPC readout and data reduction

### Implementation schemes for data readout

Due to progress in miniaturisation of electronics it is possible to consider a scenario where the front end electronics including preamp, shaper and ADC is mounted directly on the TPC (see chapter front end electronics).

From there on two alternative schemes are possible:

- the output of 128 ADC channels (of which 8–32 are integrated on one chip) is multiplexed directly (without zero-suppression) and serially transmitted to the counting house via lightfibers with 10 MB/s bandwidth. Alltogehter this would require 625 lightfibers, i.e. each padrow in every module has its lightfiber link (25 lightfibers/module). The zero suppression and some zero order filtering (at least 2 consecutive time buckets for two adjacent pads above threshold) can then be applied in a hard wired logic unit before the data are put into a buffer FIFO (10 MB to store 1 spill).

- The zero suppression as described above is already done on the detector and the output of a whole module (128 × 20 = 2560 channels) can then be multiplexed into one lightfiber link. The 5 modules closest to the beam would have to be subdivided due to the high track density. Altogether only some 30 lightfiber links would be required operating at about 3 MB/s on the average.

The final choice depends on detailed investigation of the two options. After the digital information is transmitted to the counting house the challenging task of online hit recon-

struction has to be tackled (this is a necessary feature of the data aquisition system as outlined above!). Two rather different implementations are considered here:

**Transputer array:** In this scenario the track information is read into an array of transputers, outlined in Figure 22. It is assumed, that the zero suppression is already done at the detector. The transputers were chosen (in this design) because of their excellent capability to form networks allowing a high degree of parallelism without any additional communications hard- and software.

The data rate that can be routed through the transputer links is around 1.7 MB/sec. The first level of transputers (T1...T30) would switch the information from the FIFO buffer memory to a second layer of transputers so that each transputer handles about 2 padrows of one submodule. Each of these $2^{nd}$ level transputers has a fast coprocessor, like a Digital Signal Processor (DSP) or a vector coprocessor to speed up time consumimg operations like convolutions and other matrix operations. The task would be to identify the hits and extract their $x$-$y$ coordinates and the $dE$ in each padrow. This scheme allows for easy upgrade in the case that one wants to do full track reconstruction by increasing the number of transputers. The information would be read out via a $3^d$ layer of transputers to a cluster of magnetic tape units. Assuming a computing time of 100 sec/event/transputer a total of 15 ($1^{st}$ layer) $+15 \times 10$ ($2^{nd}$ layer)$+5(3^d$ layer)$= 170$ transputers would be needed (10 events/spill).

**ASP cluster:** An alternative scheme is outlined in Figure 23. It is based on an array of Associative String Processors (ASP) presently developed by the University of Brunel in collaboration with NA35 for fast analysis of Streamer Chamber and CCD pictures.

In this scheme 4 consecutive padrows, each padrow 64 time buckets high, would be mapped into the ASP array consisting of 8 groups of Associative String Processor Elements (APEs), each group containing 8192 single ASPs, and processed simultaneously. This

mapping operation has to be repeated 7 times to cover the full range in the time direction (512 steps) and again 25 times to cover all padrows (100).

After a 2-dimensional peak finding and calculation of the peak centroids this processor array could do a local tracking in 4 planes. Preliminary estimates based on LAA benchmarks indicate a processing time of about 1msec for 4 padrows, i.e. 175ms/event. An upgrade to 7 ASP arrays, would provide a full-plane local track reconstruction in 4 padrows within 1 millisecond. It could also provide a third level trigger on multiplicity. The feasibility of the online hit reconstruction can be tested in the near future during the heavy ion run with sulfur beam in the new downstream TPC of NA35. The track density, background, diffusion etc. are very similar to the situation anticipated for a Pb on Pb experiment. Since all the raw tracking information will be written to tape in the NA35 experiment it is possible to do a thorrough off line analysis of various methods and algorithms to be developed.

## Data recording

An attractive solution for storage of the large amount of data generated even after reconstruction of the hits is the use of 8mm video cassette technology (Exabyte cassette tapes). The capacity is presently 2.5 GB. The rather slow writing speed of these units (250 kB/s) unfortunately requires the concurrent operation of several tape drives. This seems to be feasable and is planned for present experiments: Fermilab E791 for example plans to run 32 tape units concurrently.

Based on presently announced improvements this seems to become less of a problem: writing speed for Exabyte tapes of 500 kB/s and 5 GB capacity are announced for the end of this year and speeds up to 1 MB/s and 8 GB capacity are planned for the near future. Using the presently available technology and the estimate for the data flow after the first data reduction step (hit reconstruction) the task would be to write 840 KB/event for 10 events/s during a spill of 2s and a cycle of 14s (presently there exists an alternative

41

scenario with a spill of 4s and a cycle time of 19s).

Averaged over the SPS macro-cycle the data flow would then be about 2 MB/s. At 250 kb/s writing speed this would require 10 tape drives, well within reach.


## 4.3  BGO Readout

The BGO will be viewed by silicon PIN photodiodes attached to the rear $25 \times 25$mm$^2$ face. It is planned to use two $10 \times 20$mm$^2$ photodiodes held in place by a mounting fixture; this fixture will also carry a light fiber for calibration and a thermistor for temperature monitoring. We prefer to use two smaller photodiodes instead of one large one in order to have redundancy in case of failure of a photodiode (CLEO and L3 both report occasional drastic increases in leakage current of a photodiode, apparently due to epoxy problems, though this has been greatly reduced in the case of Hamamatsu photodiodes after a program of epoxy development.) This also permits mounting the light fiber between the two photodiodes, giving a better sampling of the crystal uniformity near the axis.

The photodiodes will be connected in parallel to a charge-sensitive preamplifier em-loying a FET in the input charge-sensitive loop. It will be mounted directly behind the photodiodes to minimize capacitance. The PIN diodes considered have a capacitance of 75pF/cm$^2$, meaning that a total input capacitance of 300pF will be obtained. Based on performance of similar preamps used in nuclear spectroscopy (e.g. $ORTEC\ 142B$), a noise figure of about 300 rms electrons is expected. This compares favorably with the figure of about 1500 photoelectrons released in the photodiode per MeV of energy deposited (taking light collection and photodiode quantum efficiency into account).

The signal from the pre-amplifier will the be fed to a pole-zero network and then an RC-filter network to suppress Schottky noise. This network will use either semigaussian or triangular shaping with a one or two microsecond shaping constant. We will probably use a normal trimmed pole-zero network, as the newer automatic networks may be unnecessarily

expensive. The gain of all the circuit to this point is fixed and will be monitored by means of a test-pulse input.

The photons to be detected range in energy from 50 MeV to 50 GeV, i.e. a factor of 1000. In addition, the light output from different pieces of BGO is expected to vary by a factor of two, based on L3 and low-energy nuclear physics experiences. This then requires a dynamic range of 2000, or 11 bits, in the ADC system used. And additional 7 bits are needed to handle the 1% intrinsic resolution of the BGO, and 1-2 more bits are needed to determine the photon energy within the resolution (i.e. find the centroid of a peak to better than one sigma). This requires 19-20 bits total, exceeding the capability of any present ADC. We are considering using two amplifiers separated in gain by a factor of 256 in conjunction with two 11-bit commercial ADCs, or using 6 separate amplifiers, separated by fixed factors of 4, together with individual comparators, a precision DAC and a microprocessor to build a custom ADC, one per crystal. The latter solution is similar to that of L3. It is custom but allows bringing out only a digital bus, while the former solution relies more heavily on commercial components, but requires bringing out two analog signals on coaxial cable per crystal. In principal, the latter system offers better performance when the whole range is considered.

The transparency of the BGO plus the light collection efficiency will be monitored by a light pulser brought into the crystals' back by means of an optical fiber. We plan to use our present $N_2$ laser system, which also fires all our trigger counters so that trigger timing is preserved. The light will be shifted to 480nm, the peak emission frequency for BGO, by means of a dye cell. The laser will be pulsed between spills and recorded for all crystals, as is done presently in WA80 for all photomultipliers. The gain of the electonics chain alone will be monitored every spill using a pulser which is fed to charge-sensitive preamplifiers.

The light output of BGO is very temperature dependent, quoting e.g. the L3 results, $\frac{1}{V}\frac{\Delta V}{\Delta T} \cong -1.5\%/°C$. Therefore, a thermistor will be mounted on the back of each crystal, in the same mounting fixture as carries the photodiodes, preamplifiers and optical fiber, to monitor the BGO temperature. The resistance of these will be read out by the data

43

acquisition system once per spill. By means of all these monitoring methods, we expect to be able to monitor the gain of each BGO crystal+electronics to about 0.2-0.4%. Special attention will also be given to keep the temperature stable in the detector environment.

# 5  Implementation at CERN

1. Location of the new experiment

   - The proposed experiment requests a floor area of approximately $50 \times 14 m^2$. Part of this area must be temperature controlled due to the presence of a TPC and the BGO crystals (as in L3)

   - Furthermore the location must have a clearance for beam intensities up to $1 \times 10^6$ ions/s

   - A very good shielding of neutrons from nearby beam dumps of other heavy ion experiments is required in order to reduce any disturbances due to recoil protons in the gaseous detectors.

   - The size of the proposed Large Dipole Magnet may put some further requests on the beam height dependent on its final design.

   - The present NA35 Vertex magnet will be used again, as well as the NA35 "Ring" Calorimeter.

2. Site of WA80

   The new collaboration sees the need for an early verification of the proposed trigger concept via *parallel* running of the final WA80 setup (but without the photon detectors) at the earliest lead beam time. A few days of Pb beam will allow to check the correlations:

   | | | |
   |-----|------|-----|
   | ZDC | with | $E_T$ |
   | ZDC | with | $M_c$ |
   | ZDC | with | $dN_c/d\eta$ |
   | ZDC | with | $dN/dy$ ($y < 0.6$) for protons |

   After these requested few days of Pb beam in the WA80 setup, the WA80 site is requested to be the calibration site of the new collaboration, since the newly installed

X3 high resolution line is needed for recalibration of the BGO and other detectors. The infrastructure will be all there, such as moveable mounts, a temperature controlled tent, beam and trigger diagnostics etc..

3. Construction of the Magnet (Large Dipole)

   The design of the magnet has been discussed with experts at CERN and GSI. It asks for a field of up to $\simeq$ 1.5T in a volume of ca. $2 \times 4 \times 5\text{m}^3$. The aluminum coils are to be built following the L3-magnet design and using existing tools. The total weight is expected to be between 1200 and 1500 tons. The design of the magnet should be done by CERN (with some help of GSI). The magnet infrastructure was found to be available at CERN. The construction of the coil and of the yokes are to be carried by our Indian and Yugoslavian collaborators.

4. We expect from CERN strong support in the development of the highly integrated TPC front end electronics and of CCD readout systems, some support in the development of test facilities for these chips and support in the construction of the field cage for the TPC.

5. The collaboration would like to see CERN supporting the technical implementation of the experiment on the floor and the needed high precision calibration.

6. For the most challenging problem of data acquisition we would like to have the assistance of the DD Division.

# 6  Ongoing Activities

Both the WA80 and the NA35 collaborations have ongoing $^{32}$S programs which are, however, fully in line with the R+D required for the proposed lead beam experiment. More specifically,

- a TPC is under construction to be employed next year (1990) in a S beam. This will be a milestone in the $dE/dx$ and tracking performance of a TPC.

- a BGO array is under construction for the sulphur beam in 1990.

- the construction of parallel plate avalanche detectors with optical readout to be used in the RICH detector of NA35 and the multiplicity detector in WA80 is progressing.

- laser tests with the TPC 90, especially for the development of new electronics are continuing

- the development of the Associative String Processor (ASP) of University of Frankfurt, LAA and Brunel University is aimed at an extremely efficient data compression online.

- a restructering of the WA80 data acquisition based on VME is preparing for the new detectors.

However, there is clearly the need for more manpower and the participation of new collaborations, especially from CERN, is highly desired.
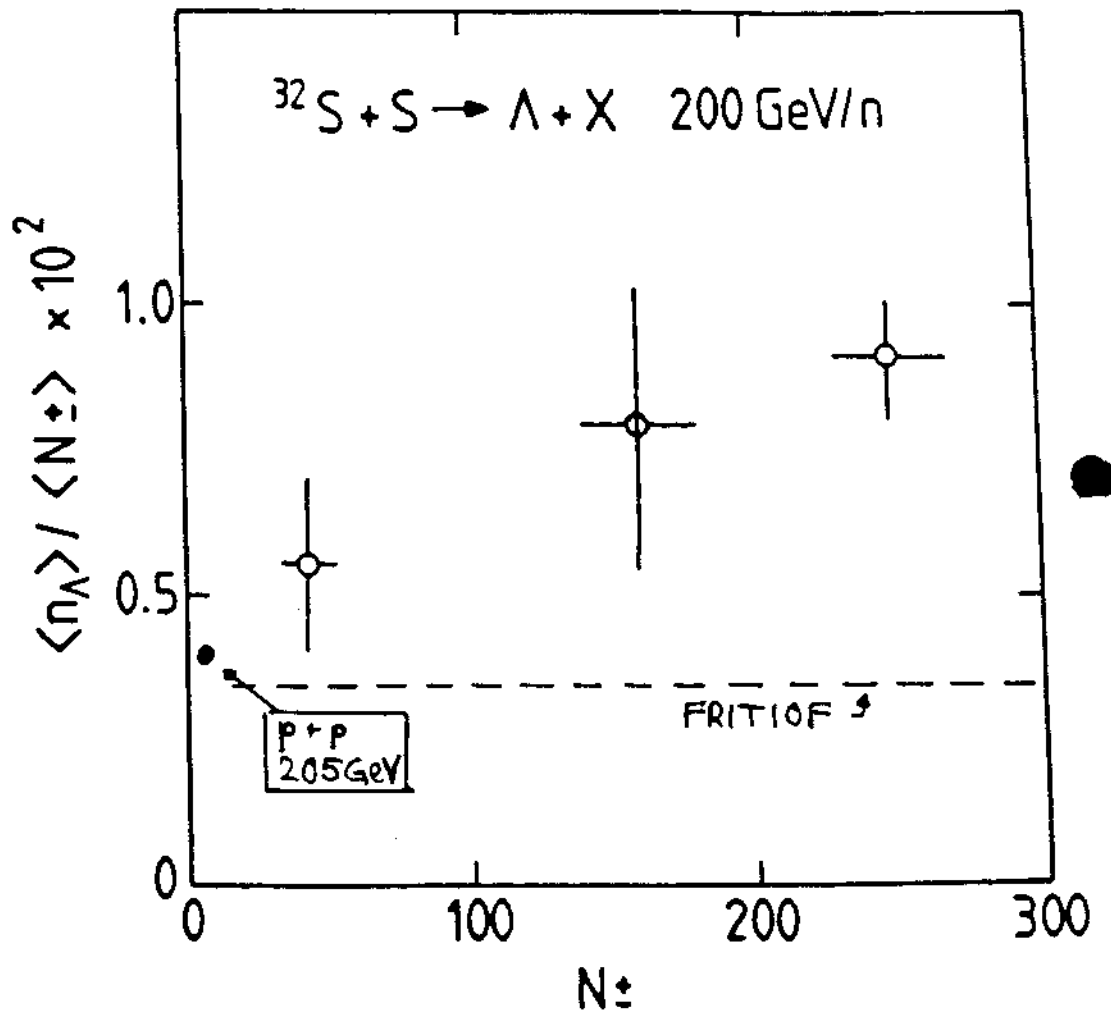
Fig. 1
Lambda to charged particle multiplicity ratio
as a function of total multiplicity ( NA 35 )

Pb + Pb 200 GeV/nucl
$2\pi^-$ correlation simulation
Single event , 1 < y < 5

Input
R = 10 fm
$\lambda$ = 0.8

Output  $\Delta p/p$ = 1.5 %
R = 10.8 ± 2.0 fm
$\lambda$ = 0.90 ± 0.2

C ($Q_{INV}$)

$Q_{INV}$(MeV)
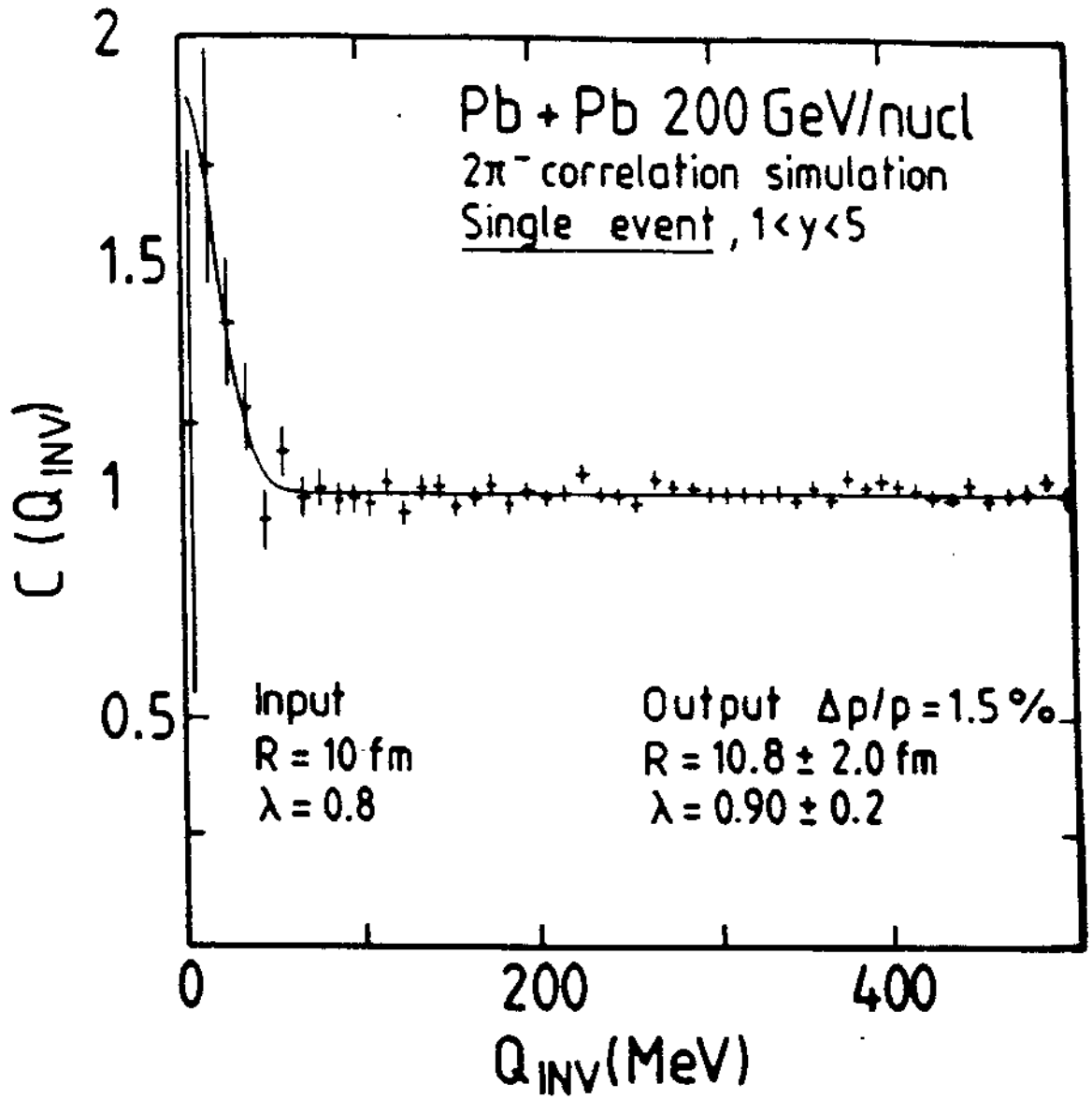
Fig.2a
Two pion correlation in a single central Pb + Pb collision
using 1000 pions as input
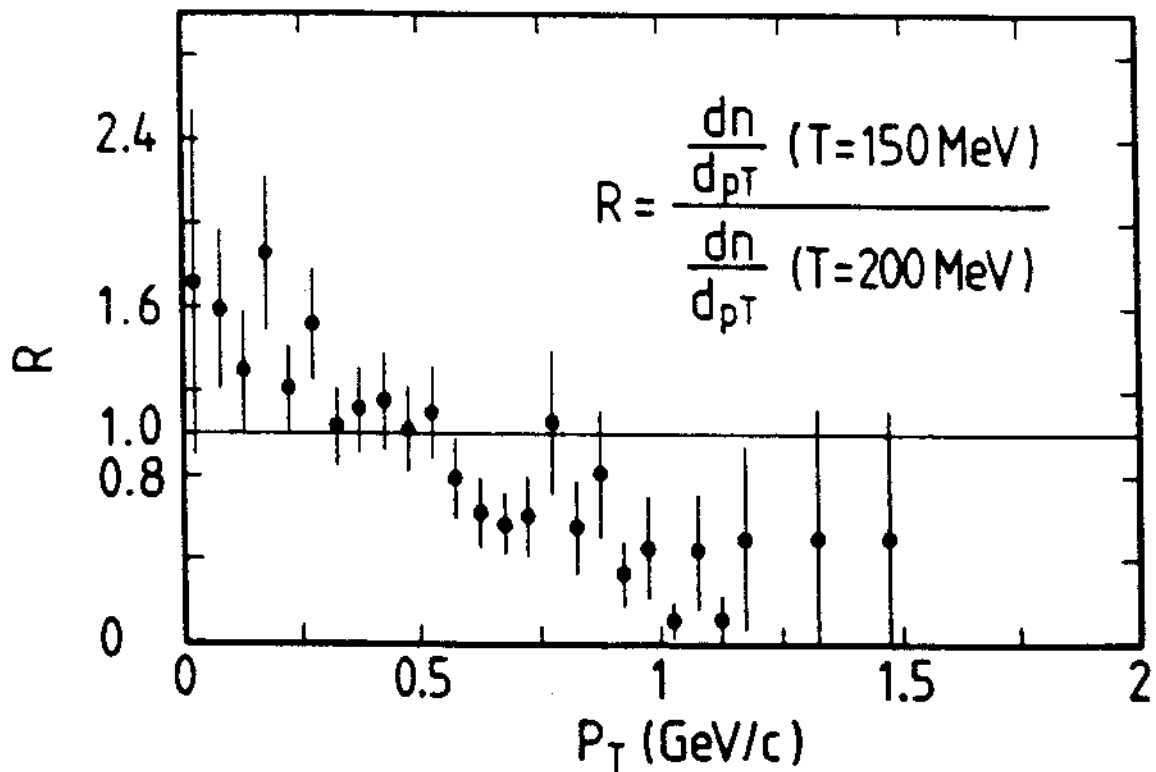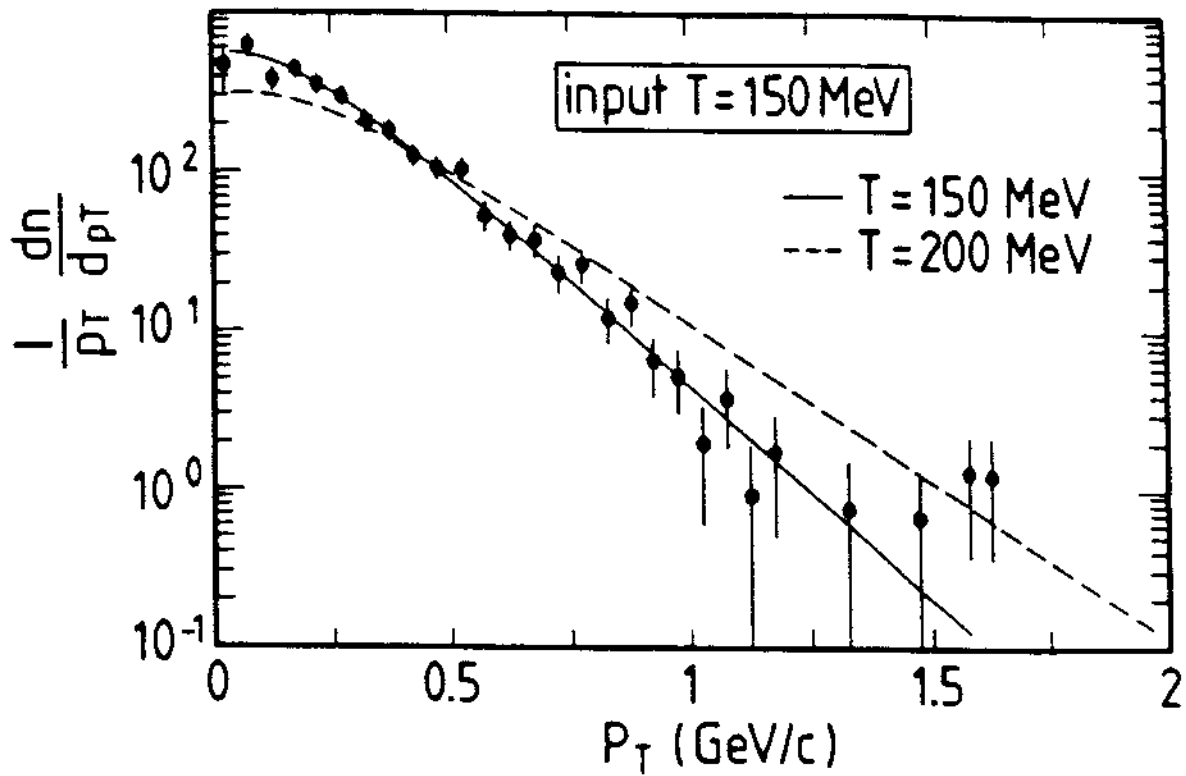
Fig.2b

Transverse momentum spectrum of pions in a single
Pb + Pb event. Monte Carlo simulation employing thermal
source of 150 and 200 MeV for 800 pions

160 A GeV Pb + Pb Fritiof, 191 project.port
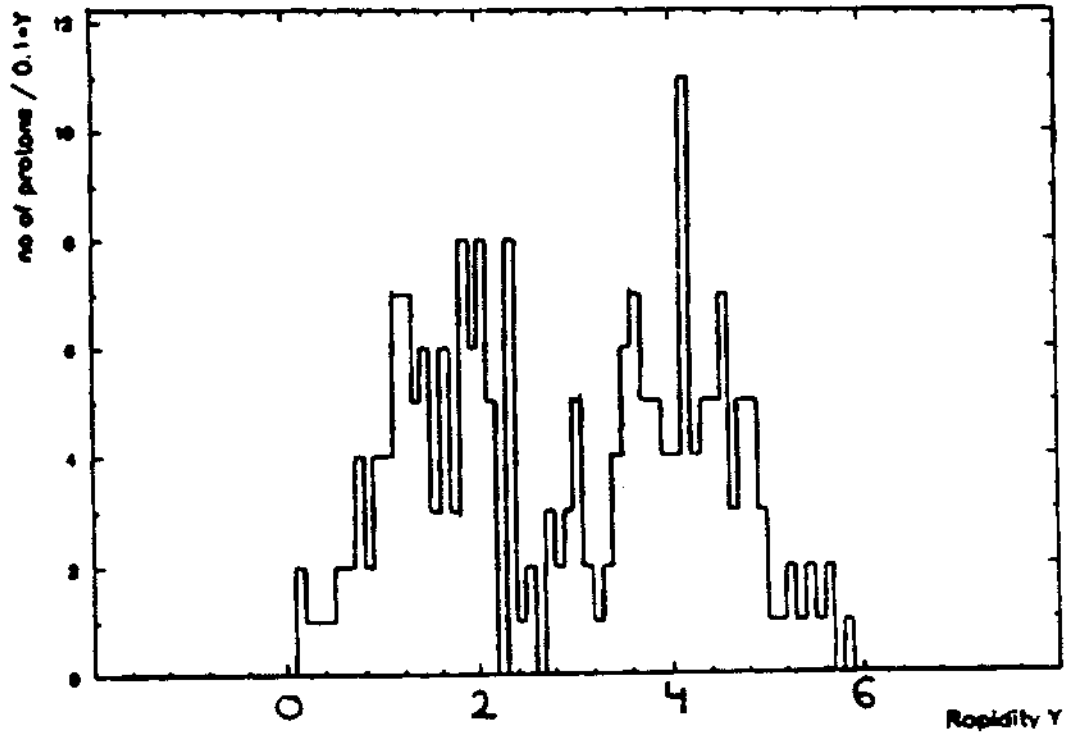
Fig. 2c

Proton rapidity distribution of a single central
Pb+Pb collision (Fritiof simulation)

# FRITIOF Pb on Pb at 160 A GeV

**GLOBAL MULTIPLICITY OF CHARGED PARTICLES**

**GLOBAL TRANSVERSE ENERGY**

**CHARGED PARTICLES**    **CENTRAL SAMPLE**
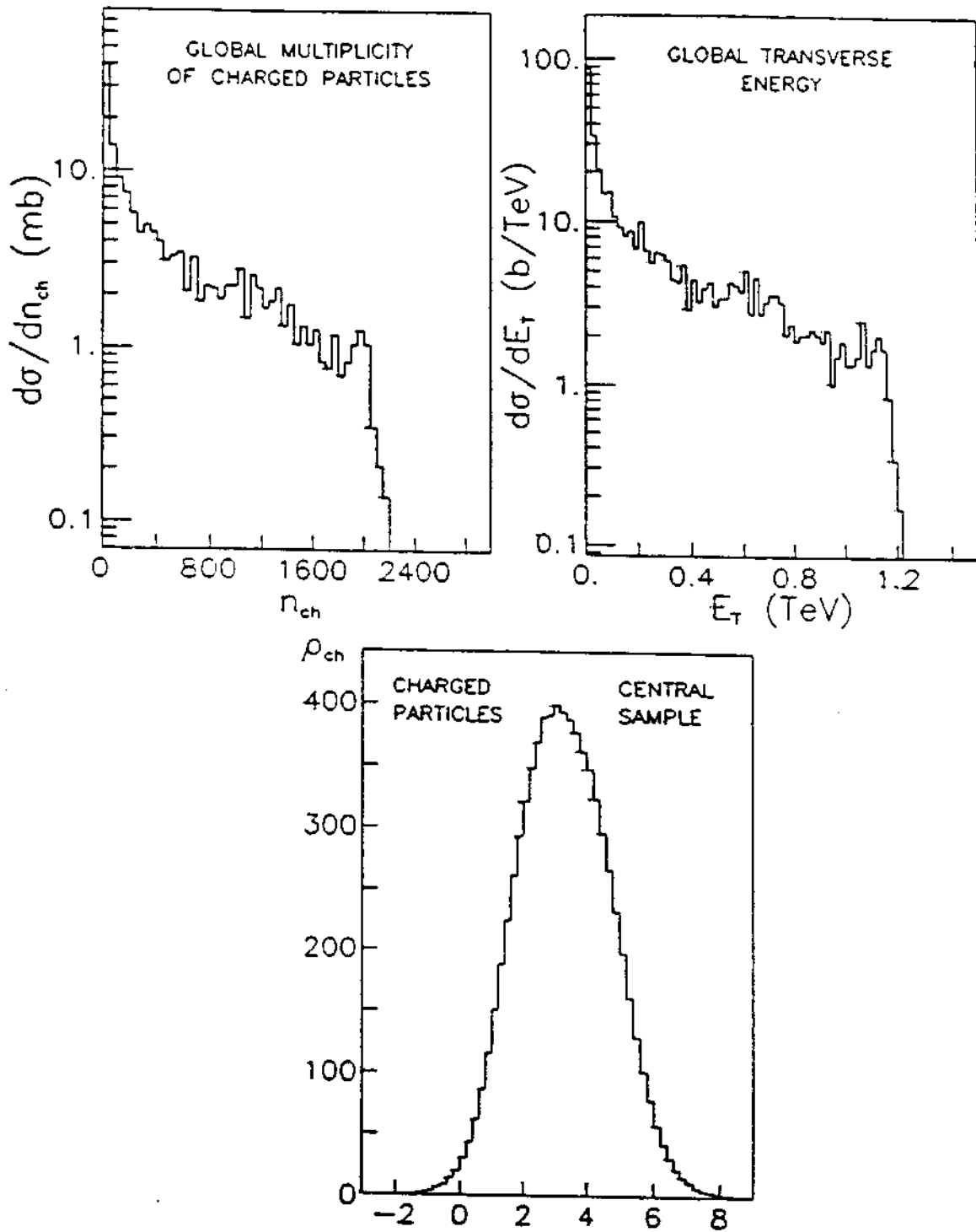
**Fig.3**

Multiplicity,transverse energy and pseudorapidity
distributions of min.bias (top) and central
(bottom) Pb+Pb collisions (Fritiof)
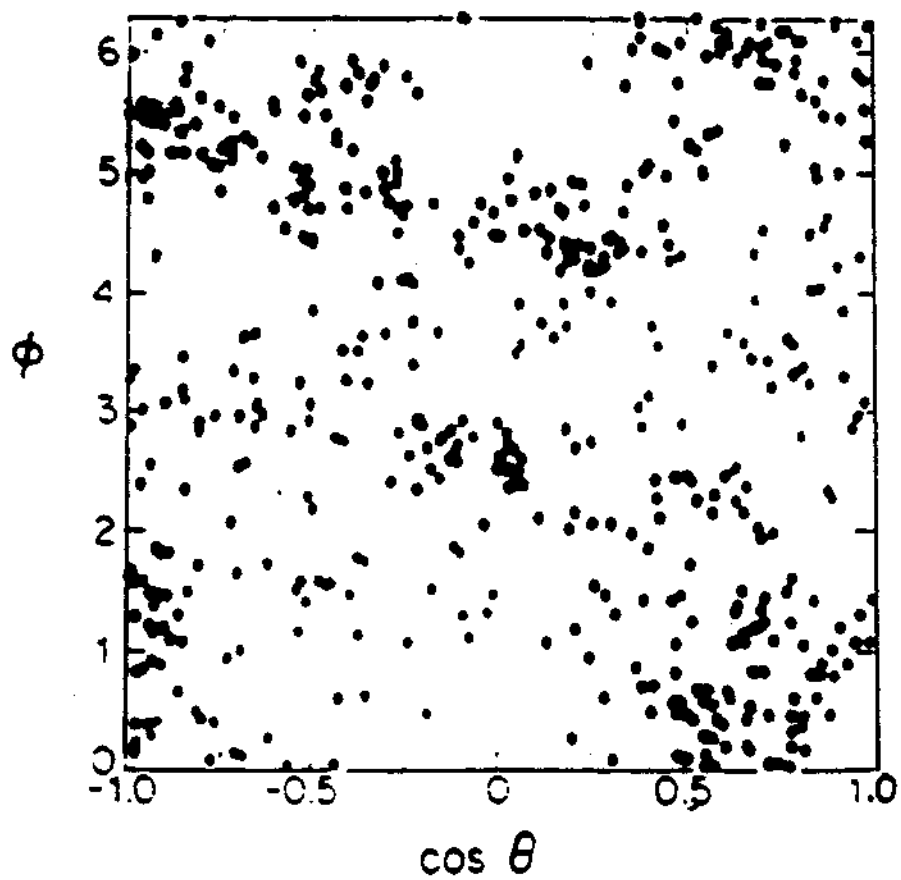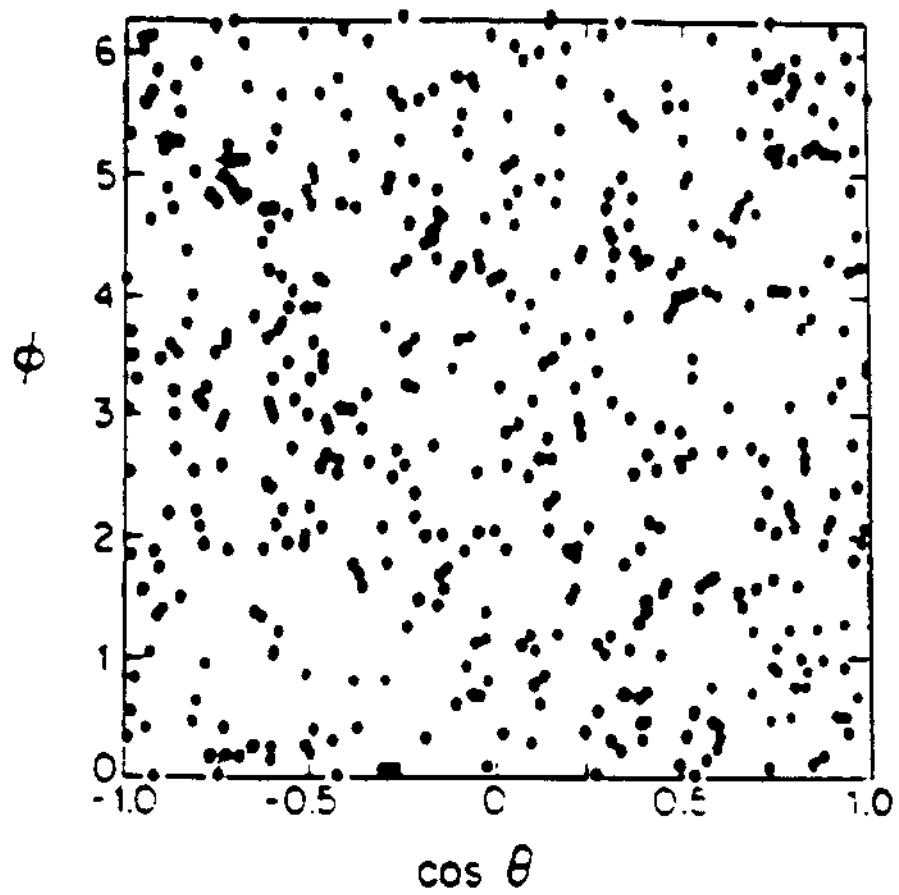
Fig.4  500 like-sign pions in configuration space with
(bottom) and without Bose-Einstein correlation
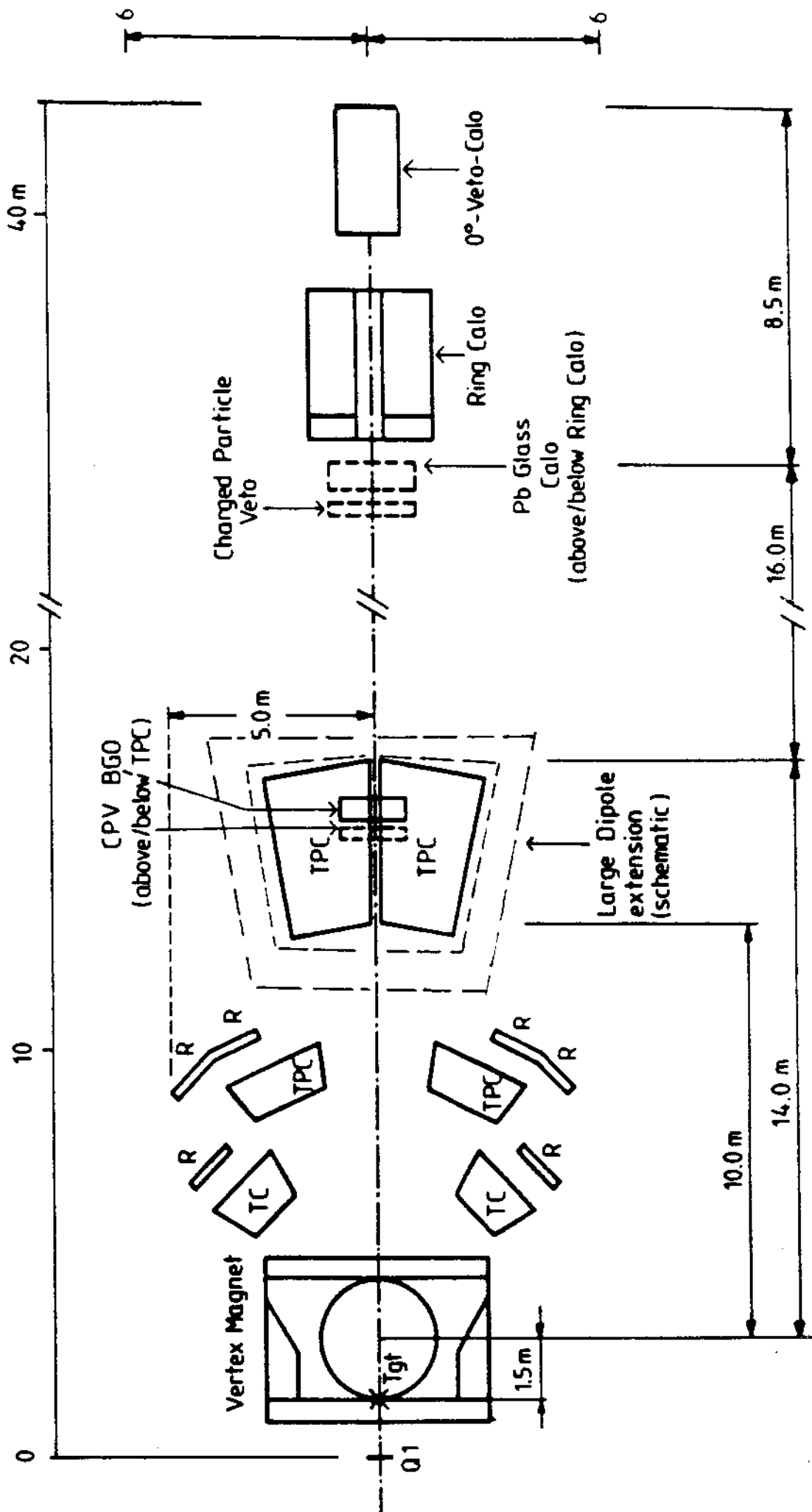
Fig. 5
Large Acceptance Hadron and Photon Experiment layout

All Charged Particles

X vs Y at 10 m
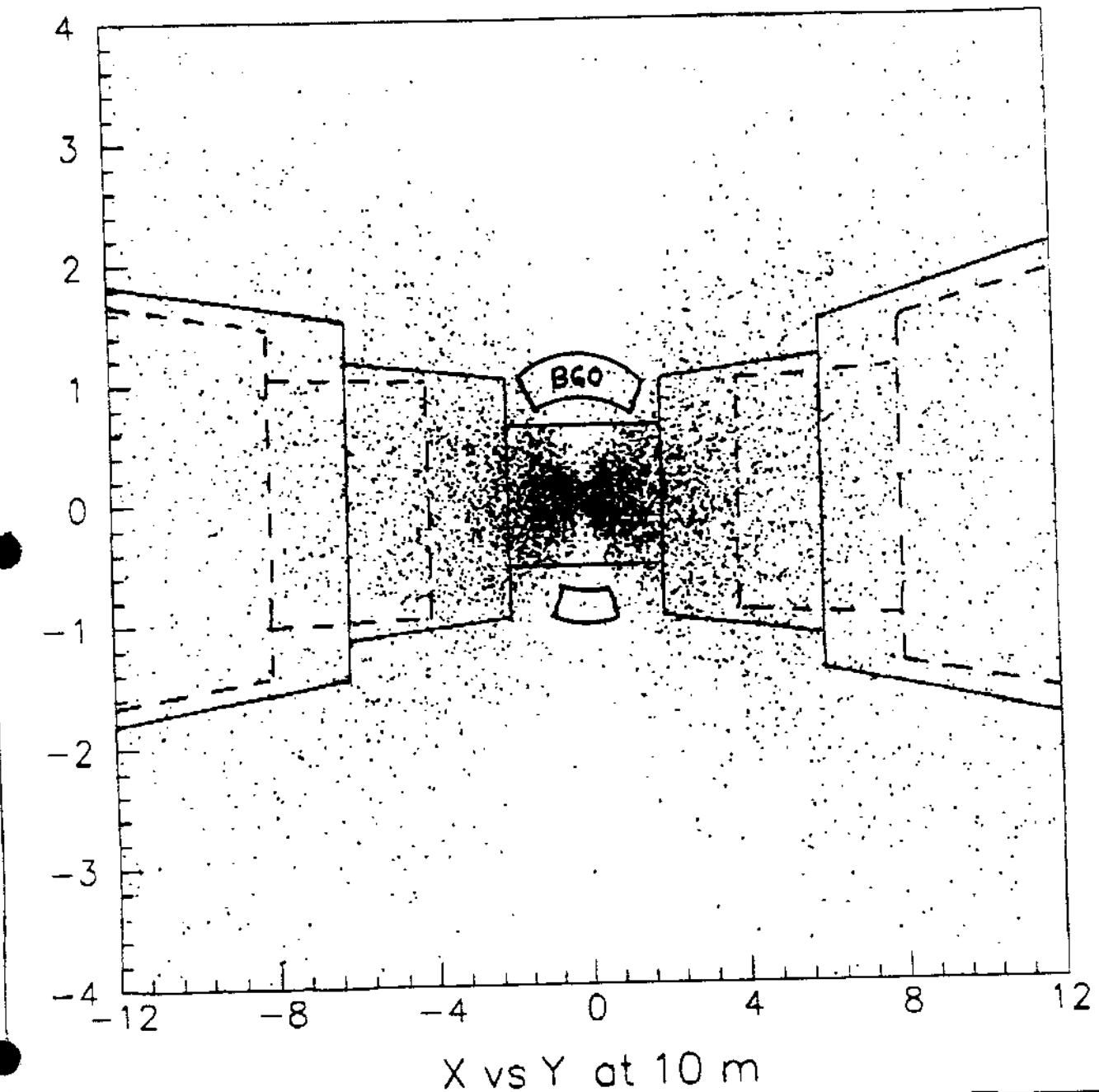
Fig.6
Active area of the central and lateral TPCs,
the RICH detectors (dashed) and the BGO arrays,
as projected onto a plane 10m downstream of the
magnet center, superimposed on ch. particle hit
pattern

**Relativistic Rise for Ne + 10% C2H6 (1 atmos.)**

Data from Lehraus et al. IEEE Trans. Nuc. Sci. NS30, 50 (1983)
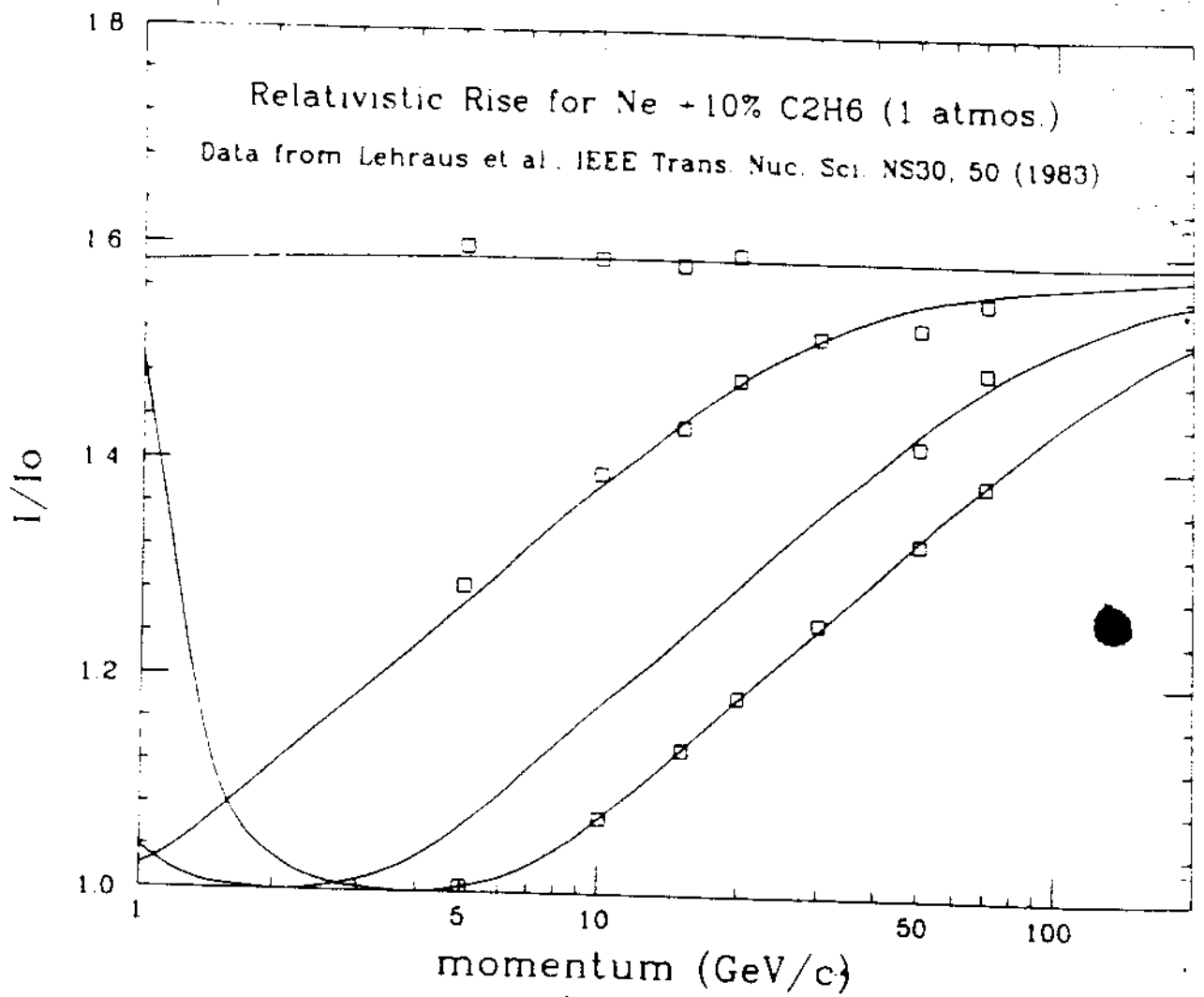
Fig.7

Specific ionization in Ne gas for pions, kaons and protons, as function of momentum
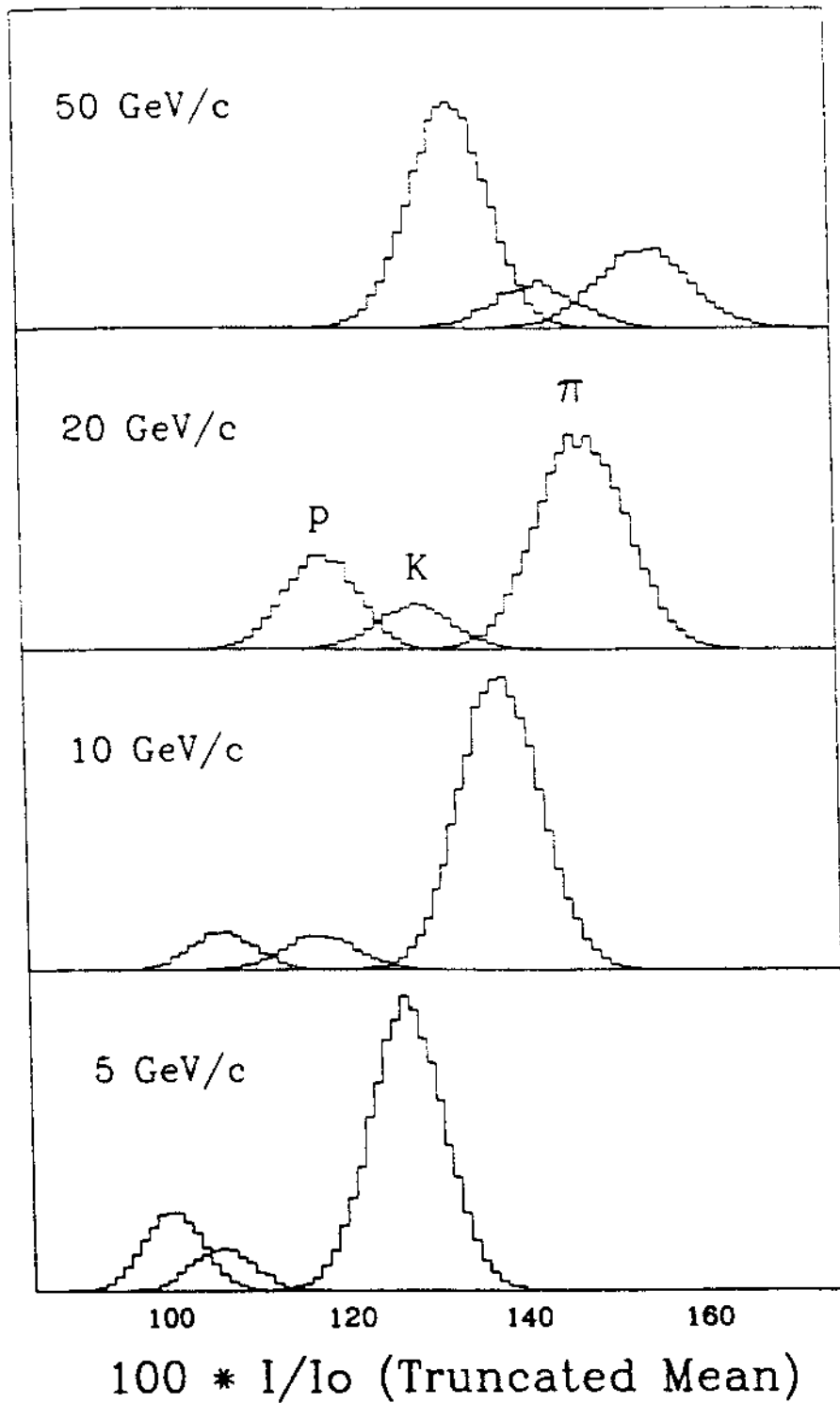
Fig.8

Ionization spectra of pions, kaons and protons
at various lab. momenta expected for the central TPC

5.0 GeV/c

π

p

K

3.0 GeV/c
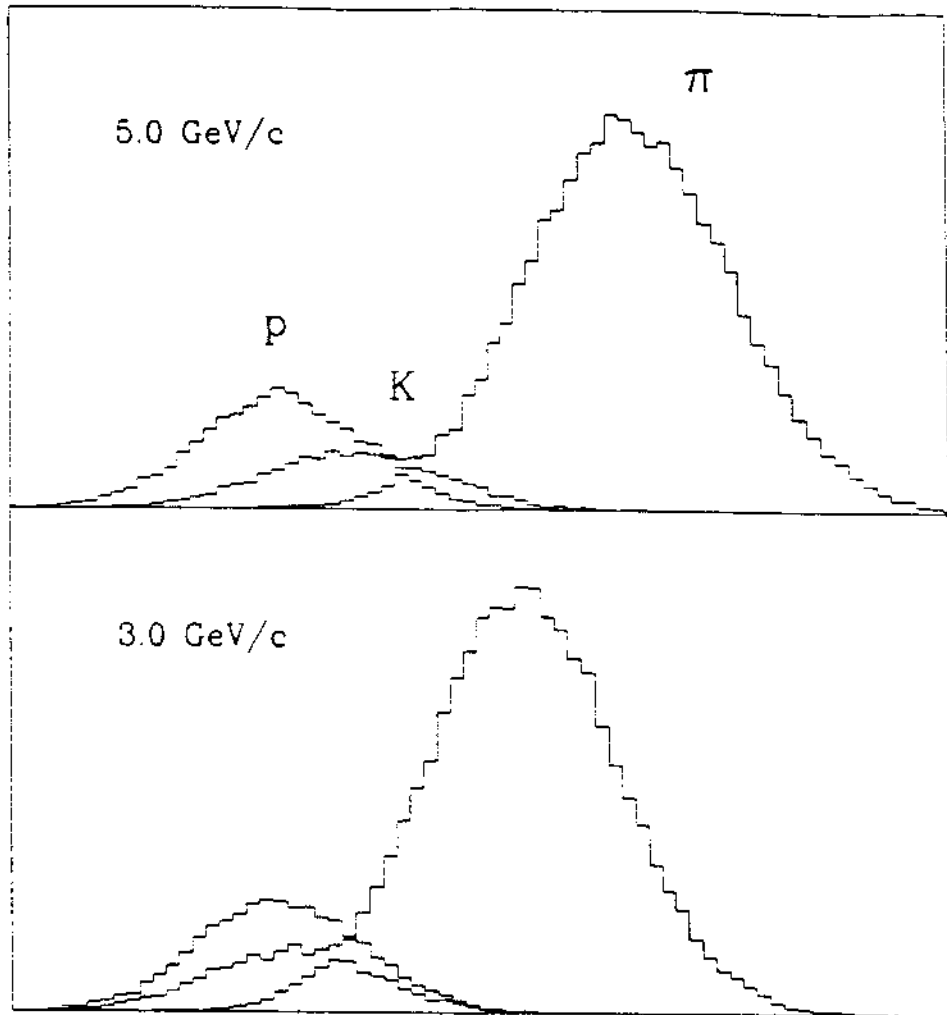
Truncated Mean 100 * I/Io

Fig.9

Ionization response for 1.2m TPC ,for pions, kaons and protons
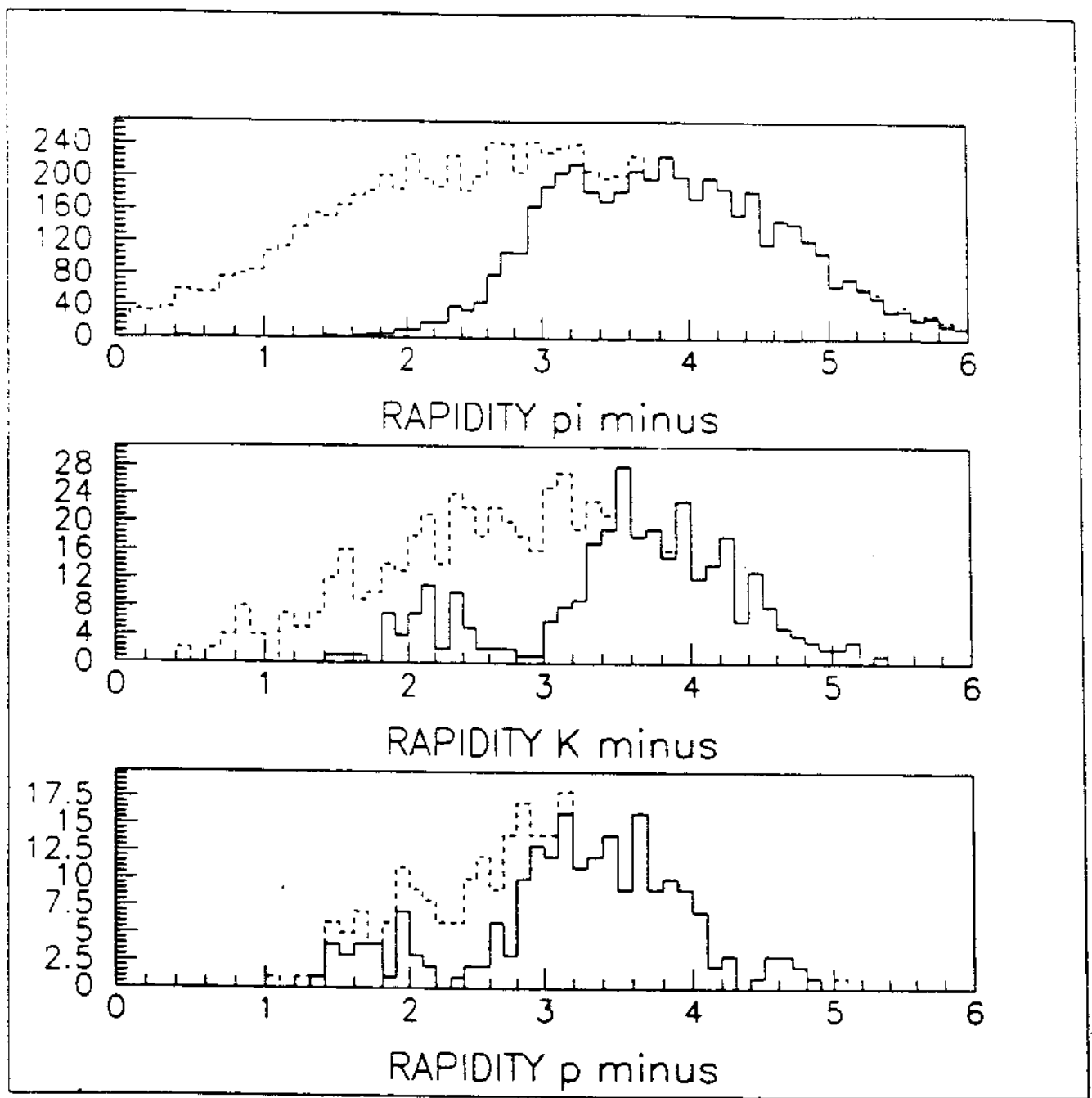
Fig.10
Rapidity distributions of identified neg. pions, kaons and
antiprotons, compared to the total yield (Fritiof)
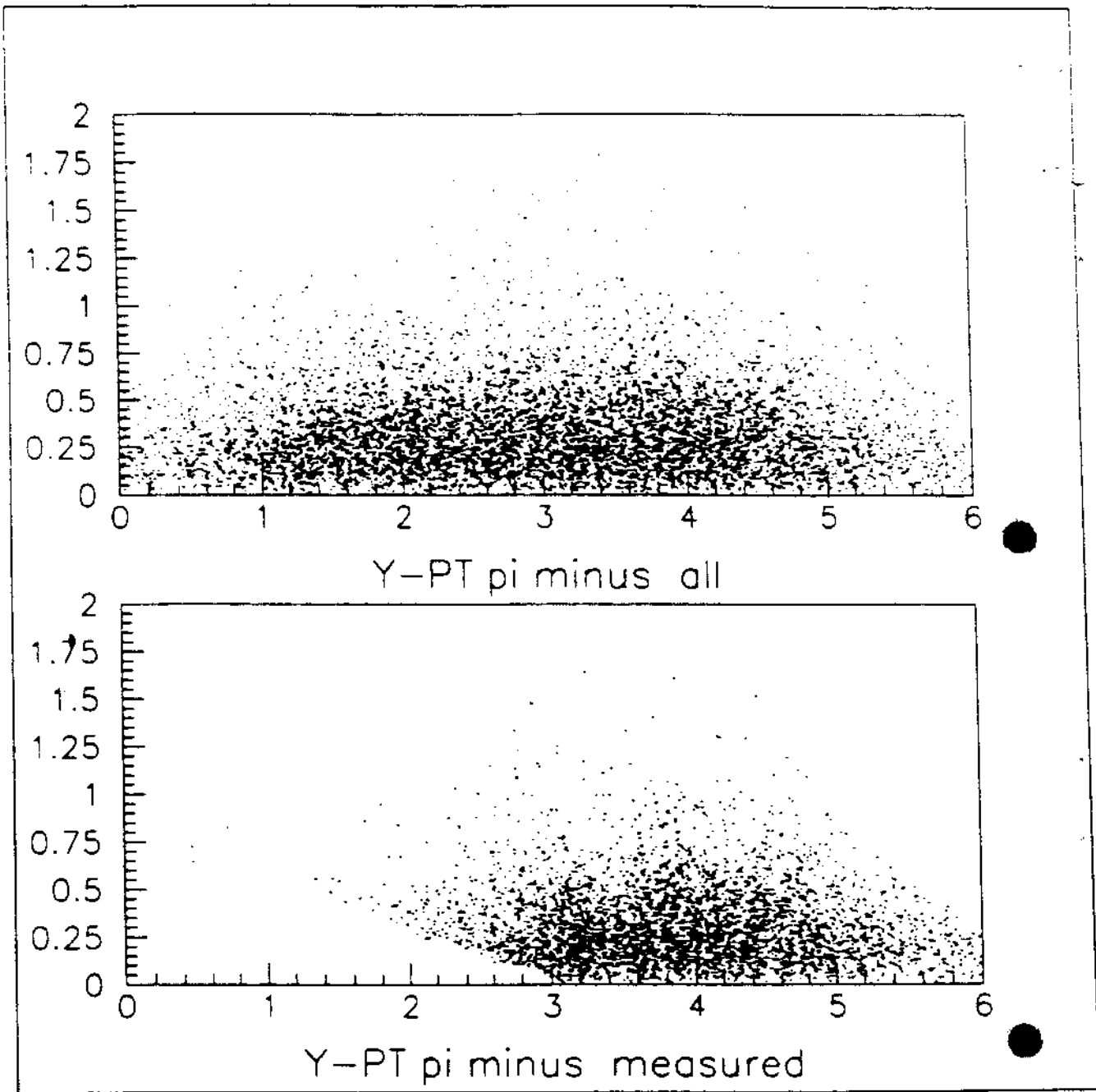
Fig. 11

Rapidity vs $p_t$ scatter plot of central Pb+Pb collision
pions showing total and identified fractions (TPCs and RICH)
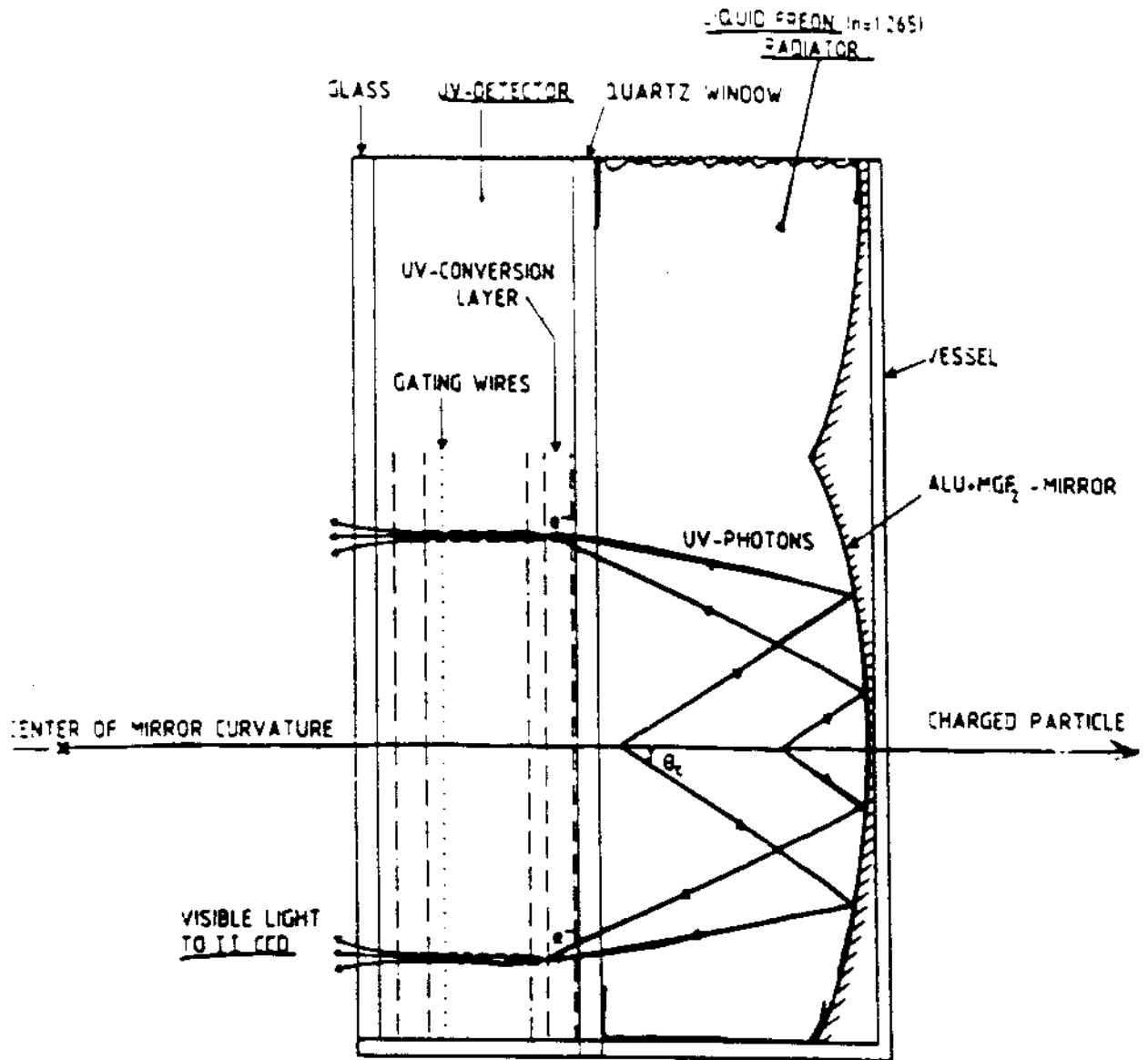
Fig.12

Structure of the RICH detector with incident char-
ged particle traversing the UV detector section
before entering the (liquid Freon) radiator- and
imaging mirror section

Y-PT-PIONS



Pion acceptance

Y-TOTAL-PIONS
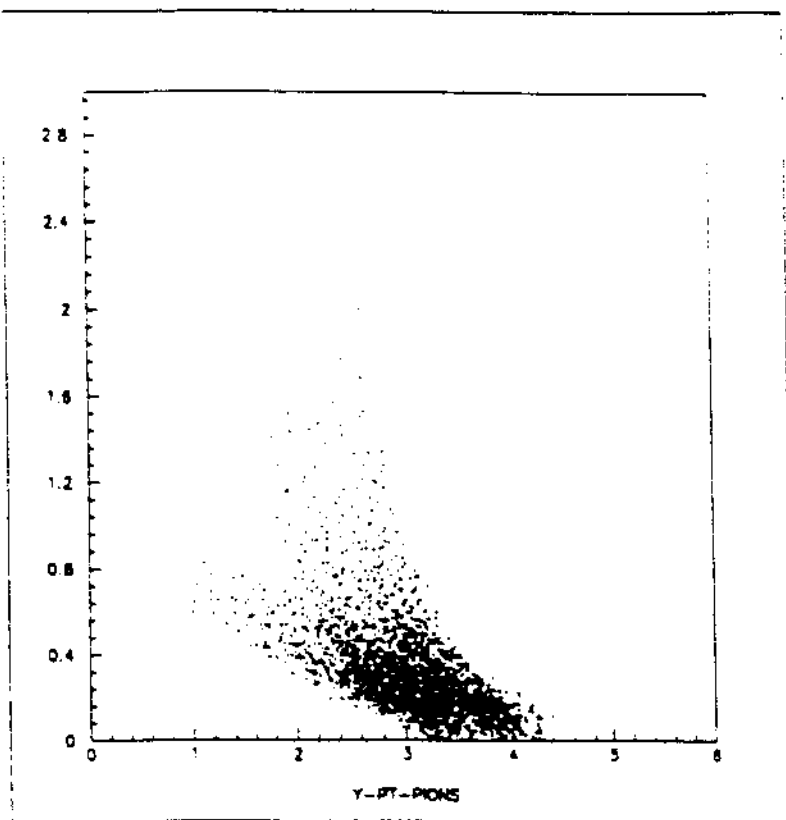
Fig.13

Pions accepted by the
RICH detector shown in
$y$-$p_T$ scatter plot and
in the rapidity spec-
trum (Pb+Pb Fritiof)
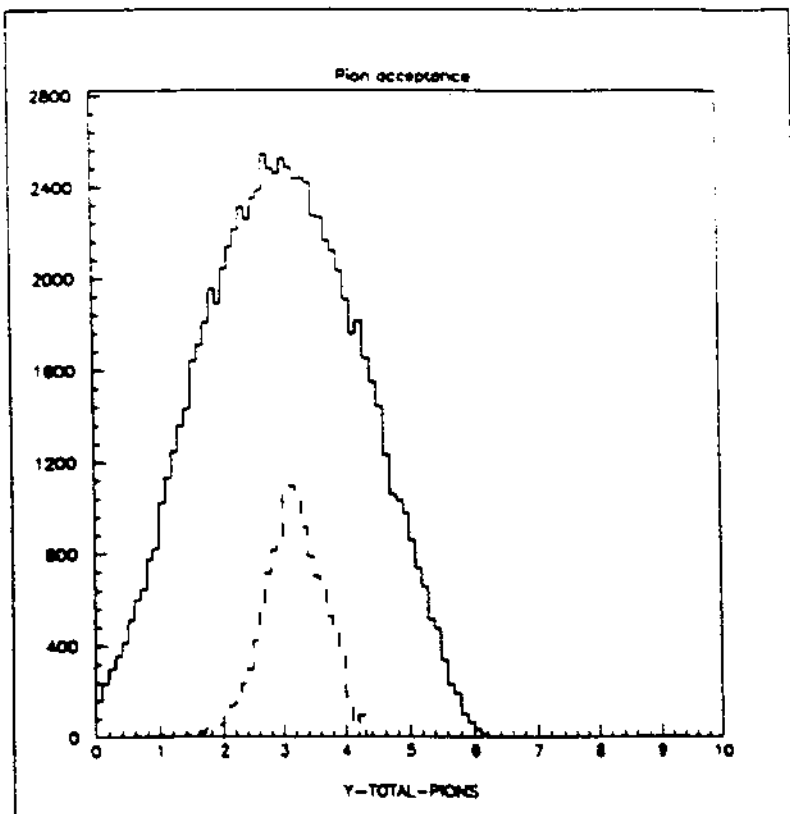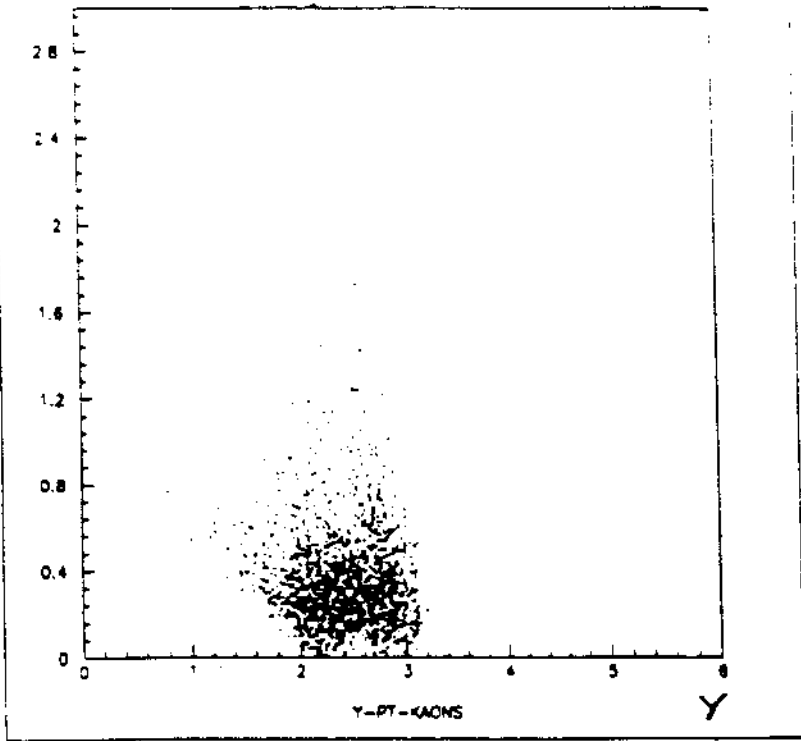
Fig.14
RICH acceptance for kaons (top) and protons (bottom) in $y$-$p_t$ plane (Pb+Pb Fritiof)
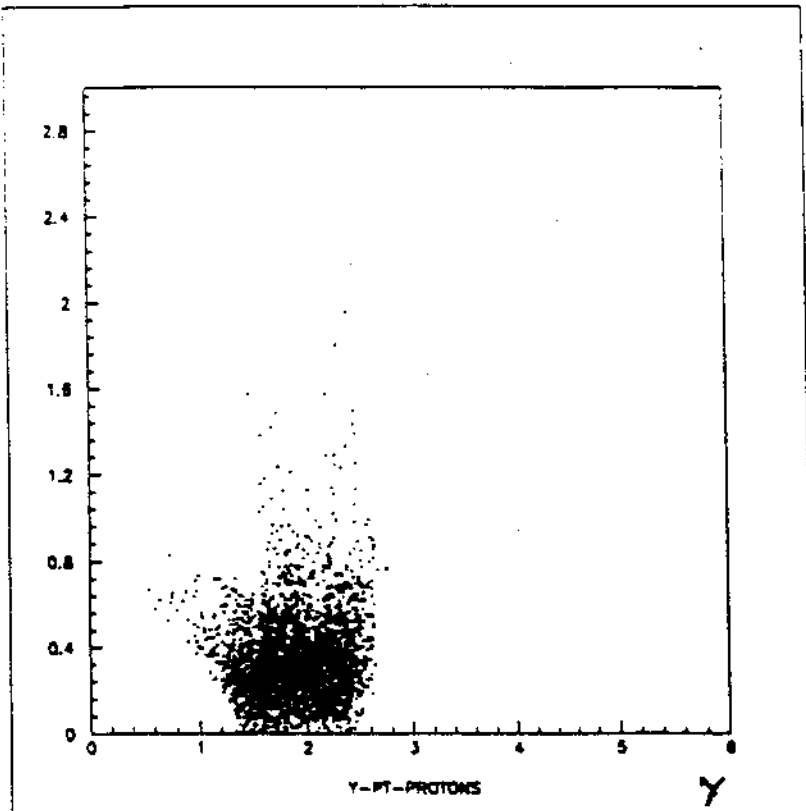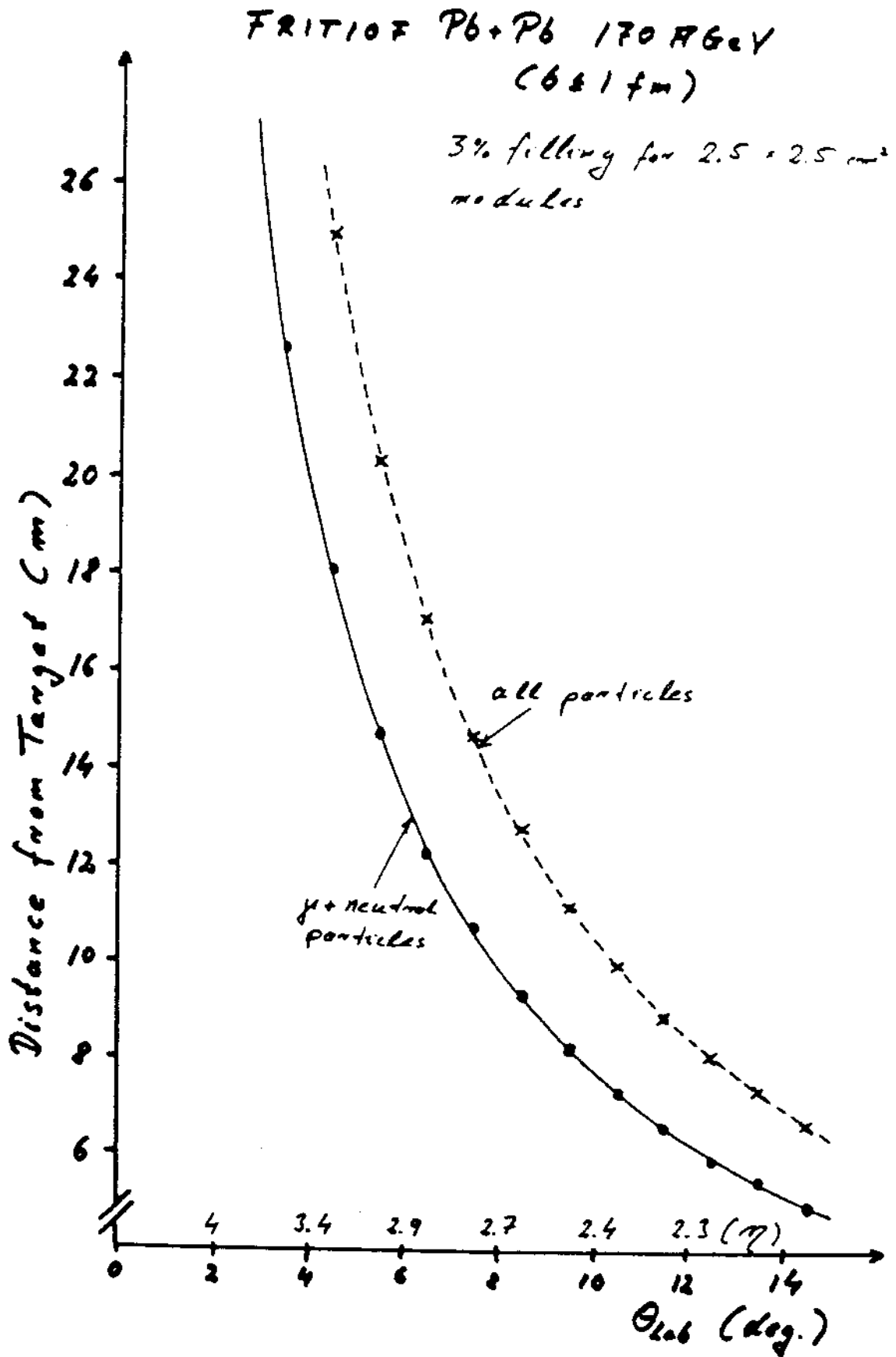
Fig.15: Position of a BGO detector from the target,where
less than 3% of all BGO modules are hit by particles
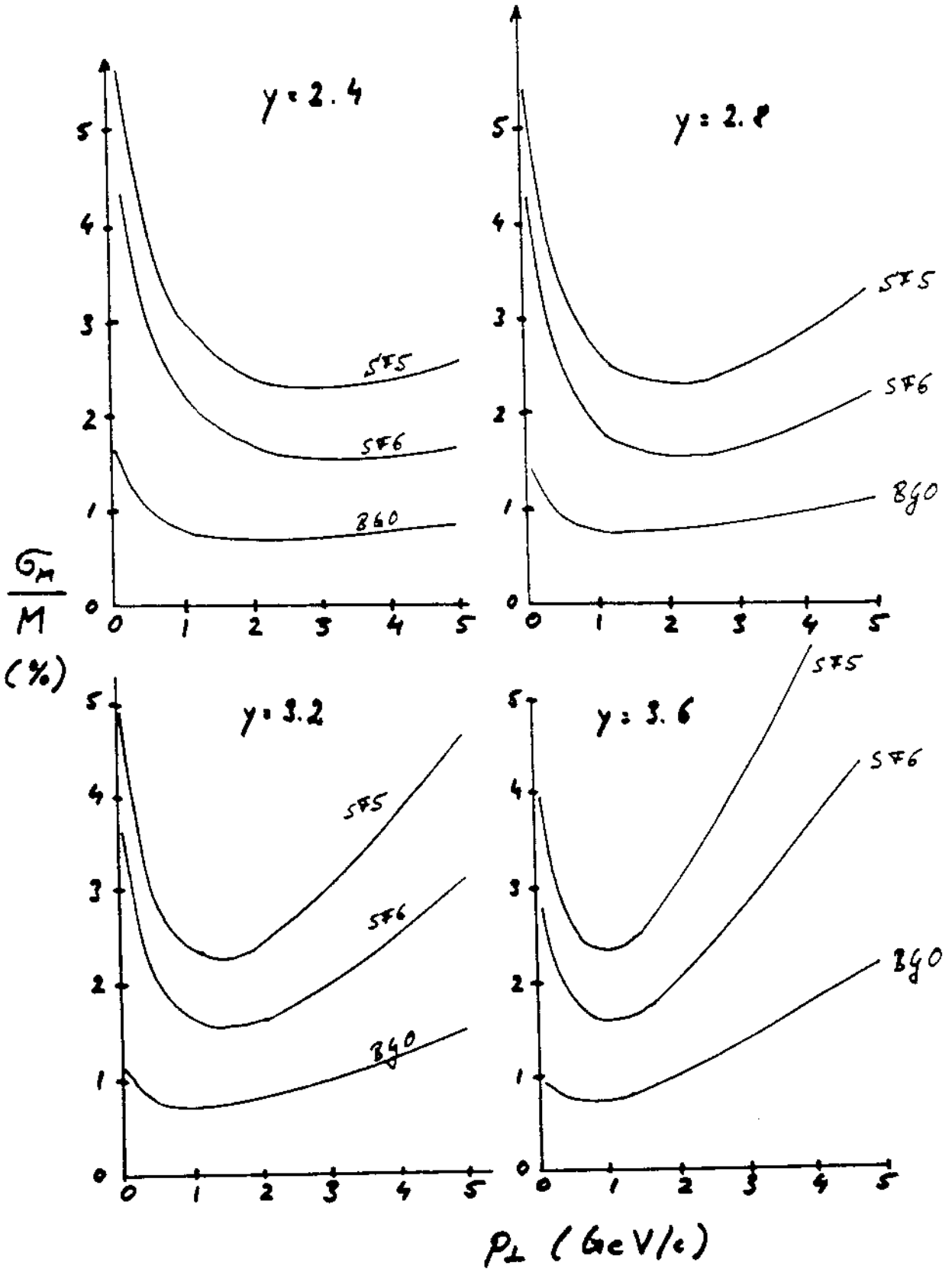
Fig.16a: $\pi^0$ mass resolution for different detectors of BGO, SFS and SF6 Leadglass

# η Mass Resolution (α < 0.5)



Fig.16b: η mass resolution for different detectors of BGO,SF5 and SF6 Leadglass

160 A GeV Pb + Pb  BGO 12000 FRITIOF

4.4–5.7° $\Phi=26-106$, $176-216$  $E_\gamma>.05$

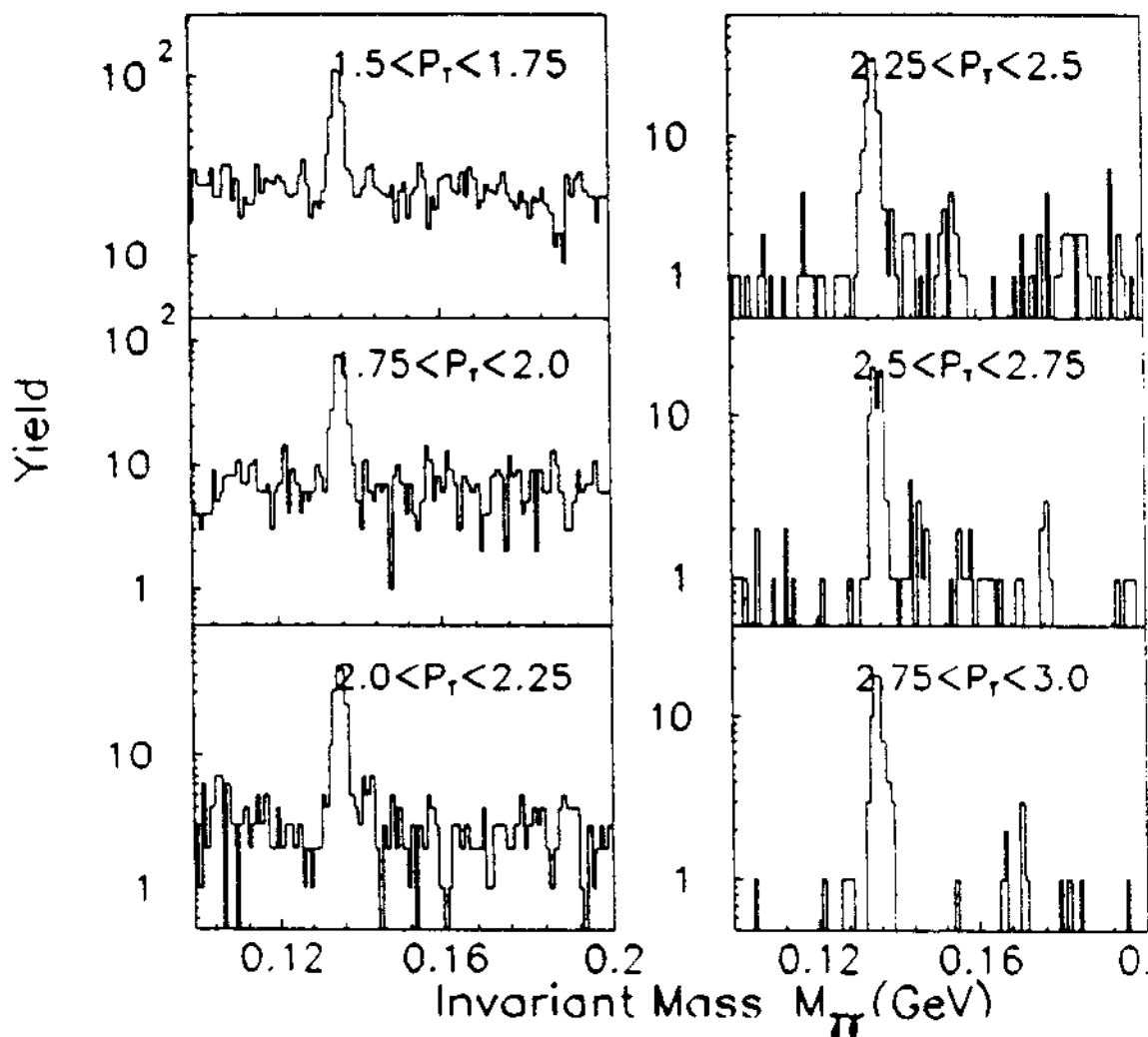$\delta E=.01E+.0\sqrt{E}$  $\delta x=2.9/\sqrt{E}+.1mm$  $\alpha<0.5$
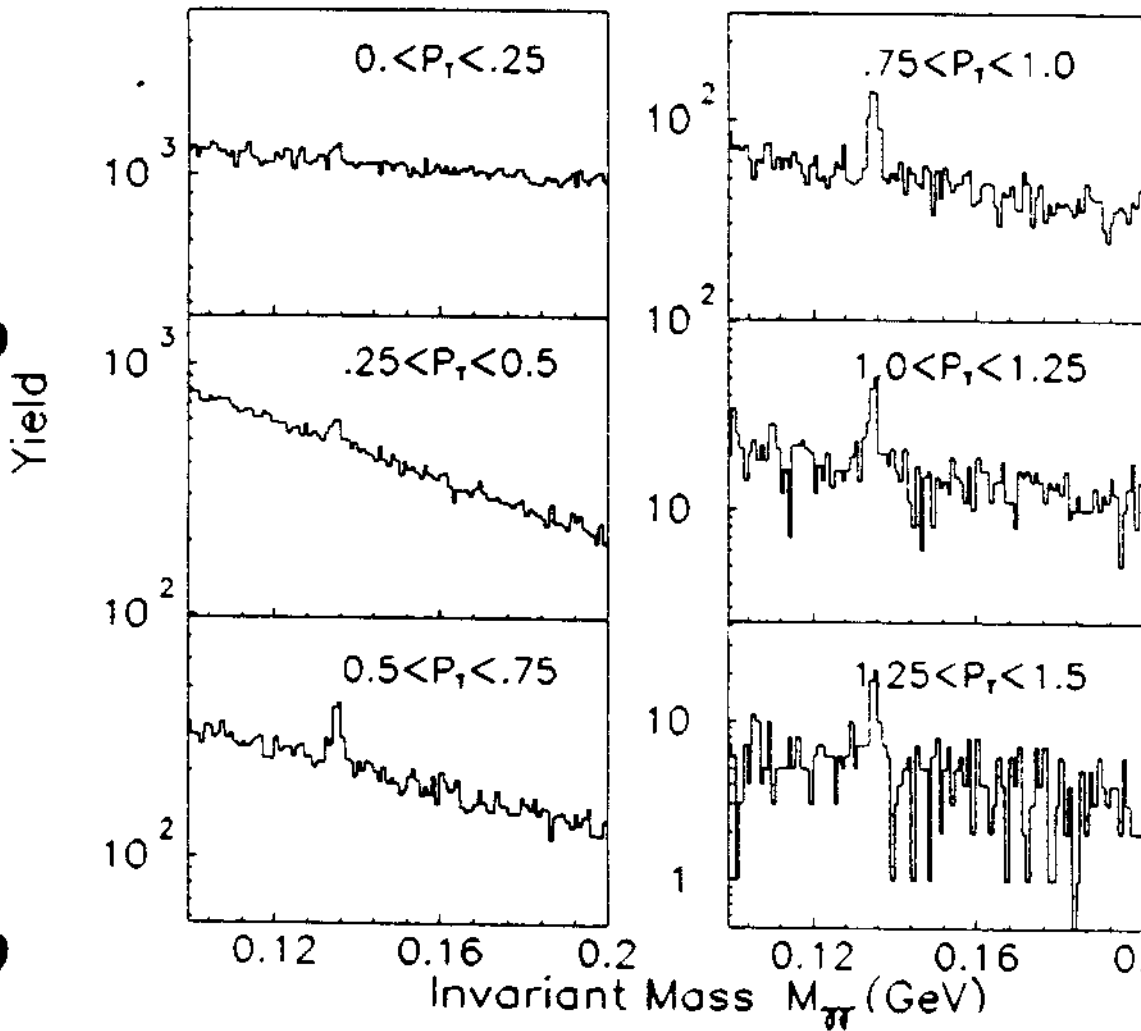


Fig.17: Invariant mass spectrum of two photons in different $P_\perp$- windows in a BGO detector for minimum bias events

# 160 A GeV Pb + Pb  SF5 12000 FRITIOF
## 3.5−4.4° Φ=0−106, 176−282  $E_\gamma$>0.4
## $\delta E$=0.06√E+.004E $\delta x$=5.0mm  α<0.5



Fig.18: Invariant mass spectrum of two photons in different
$P_\perp$ - windows in a SF5 detector for minimum bias events

160 A GeV Pb + Pb  BGO 25000 Central Monte
4.4-5.7° Φ=26-106, 176-216  E,>.05
δE=.01E+.0√E δx=2.9/√E+.1mm α<0.5



Fig.19a:Invariant mass spectrum of two photons in different
$P_\perp$- windows in a BGO detector for central events only

160 A GeV Pb + Pb  BGO 25000 Central Monte
4.4-5.7° $\phi$=26-106, 176-216  $E_\gamma$>.05
$\delta E$=.01E+.0$\sqrt{E}$ $\delta x$=2.9/$\sqrt{E}$+.1mm $\alpha$<0.5

Fig.19b:Invariant mass spectrum of two photons in different
$P_\perp$- windows in a BGO detector for central events only

160 A GeV Pb + Pb  SF5 25000 Central Monte

$3.5-4.4°$ $\phi=0-106$, $176-282$  $E_T>0.4$

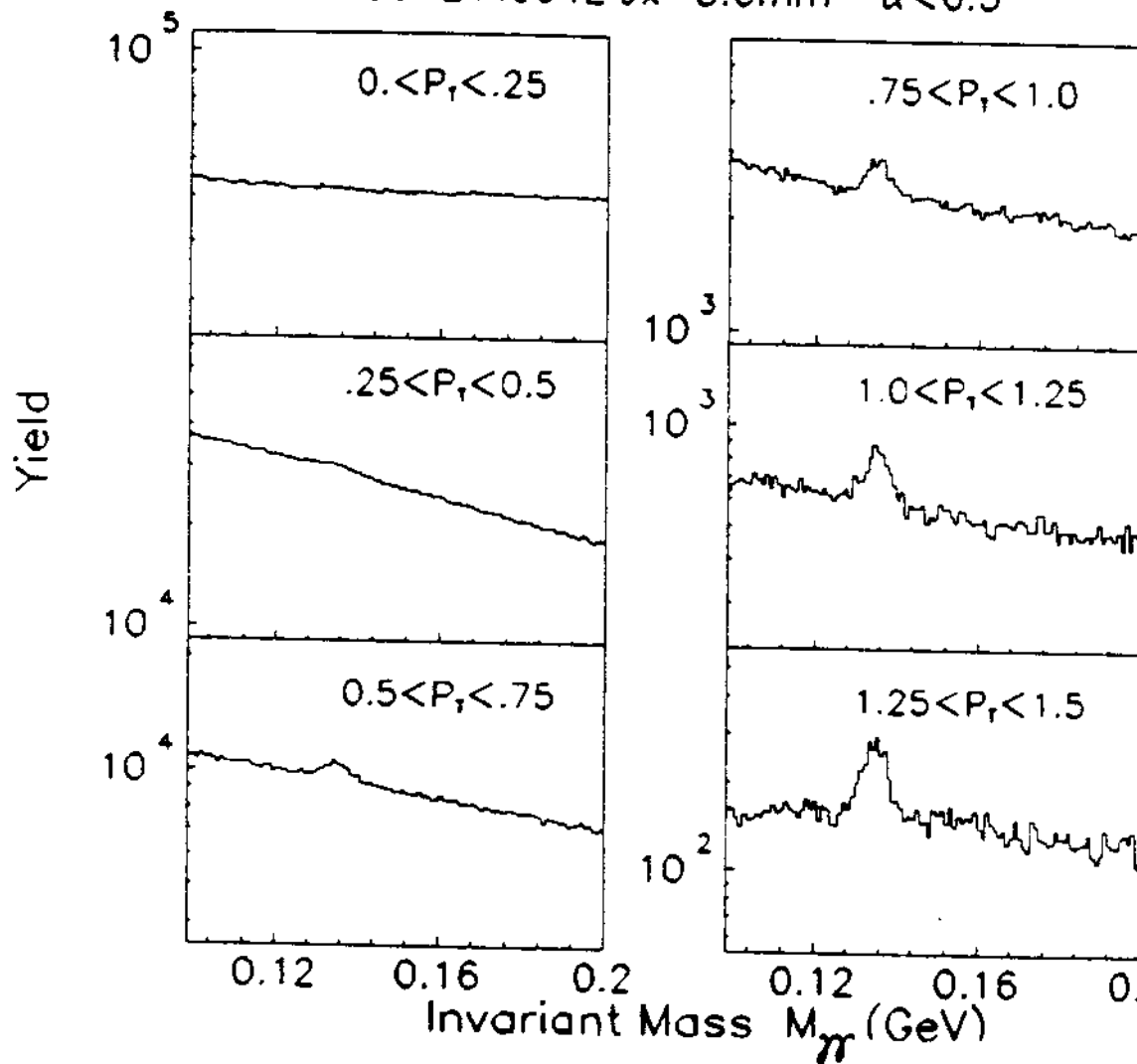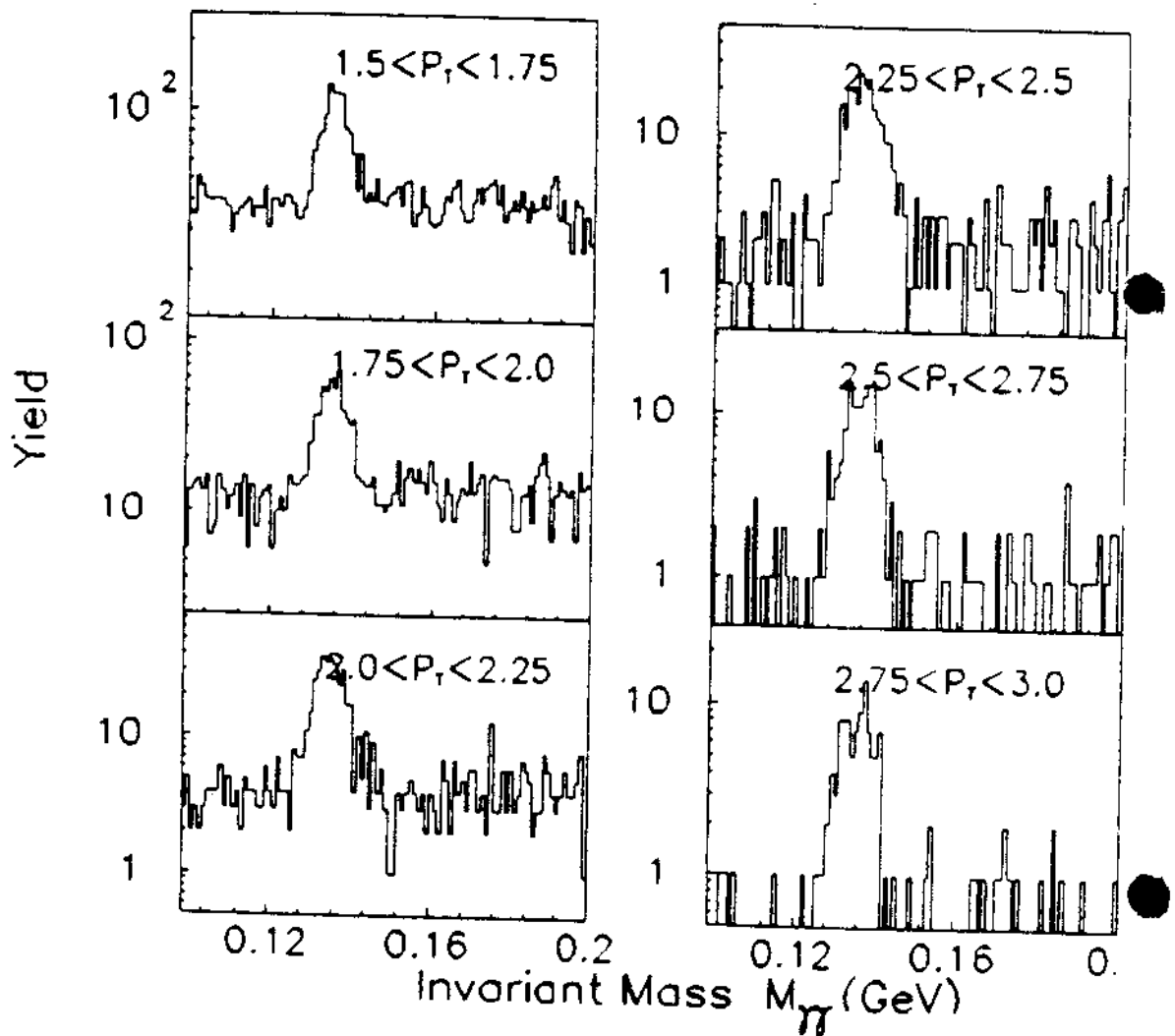$\delta E=0.06\sqrt{E}+.004E$  $\delta x=5.0mm$   $\alpha<0.5$



Fig.20a: Invariant mass spectrum of two photons in a SF5
detector for different $p_\perp$-windows and central events

160 A GeV Pb + Pb  SF5 25000 Central Monte

3.5-4.4° Φ=0-106, 176-282  $E_\gamma>0.4$

$\delta E=0.06\sqrt{E}+.004E$  $\delta x=5.0$mm   $\alpha<0.5$

Fig.20b: Invariant mass spectrum of two photons in different $P_\perp$- windows in a SFS detector for central events only
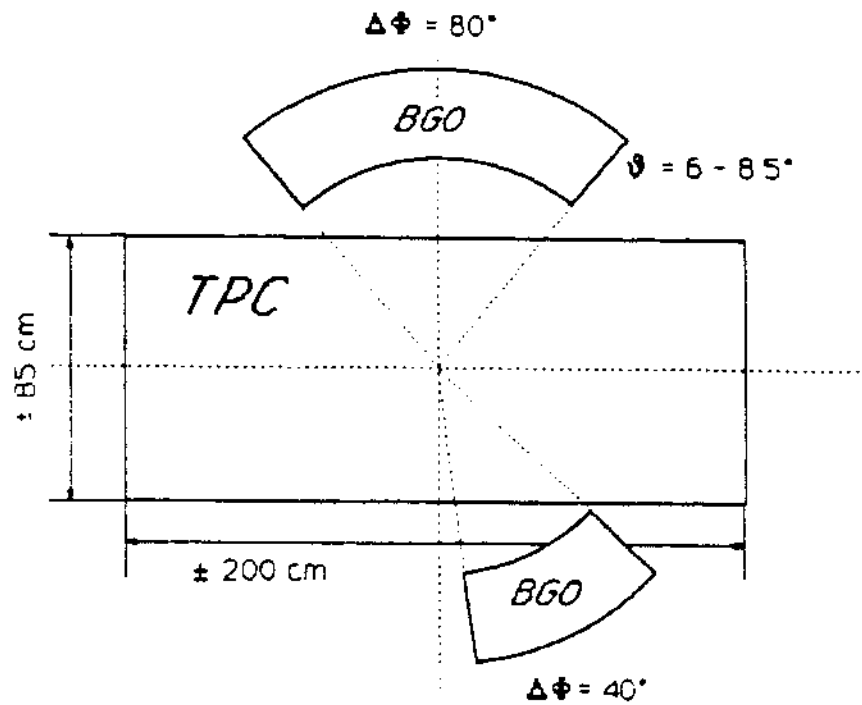
# Projected view from target (cut at 13 m)



Fig.21: Azimuthal positioning of the two BGO detectors with respect to the TPC

# TPC FRONT-END ELECTRONICS
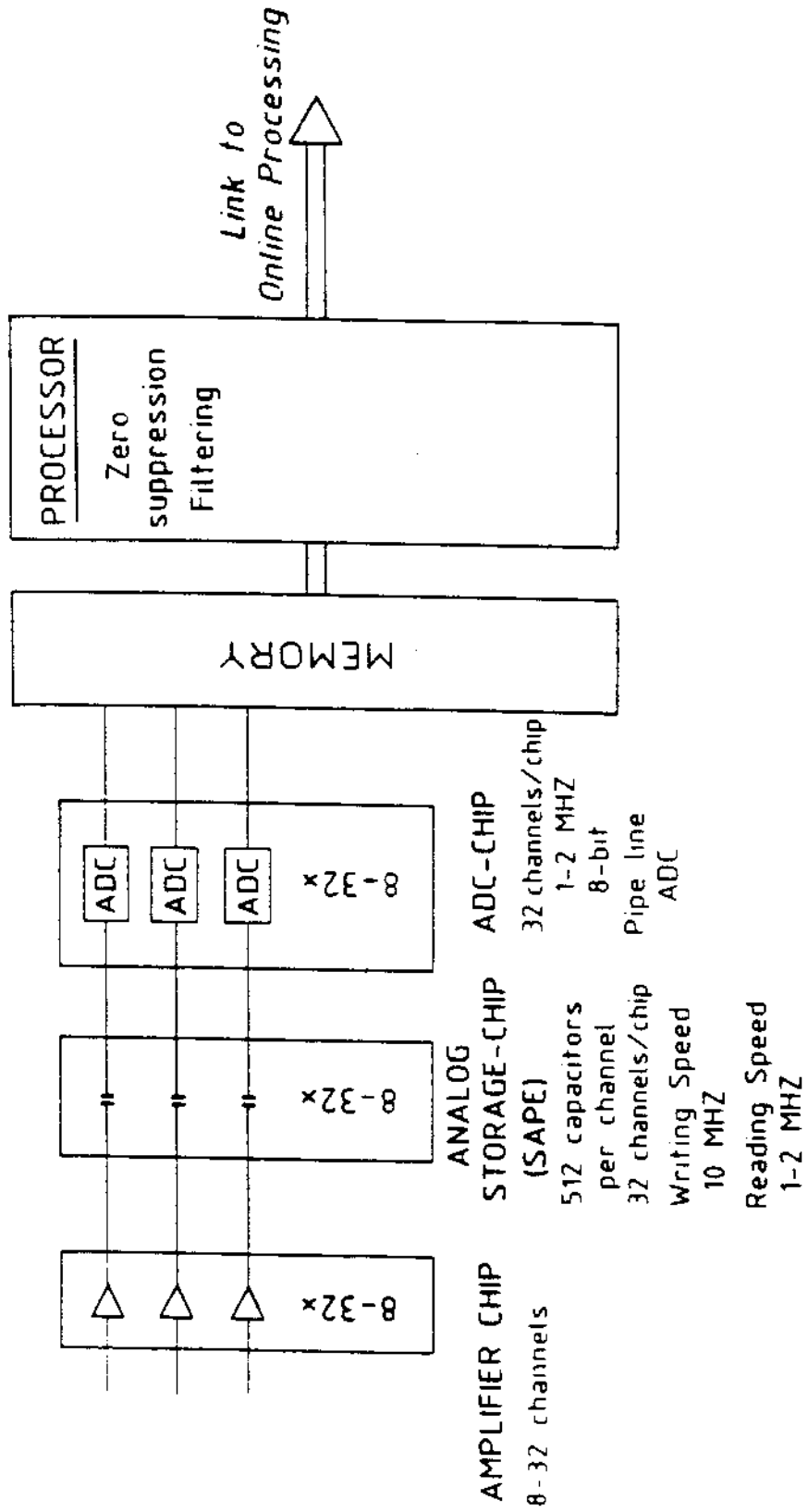## CONCEPTUAL DESIGN

PROCESSOR

Zero suppression
Filtering

MEMORY

Link to
Online Processing

8-32×   8-32×   8-32×

ADC
ADC
ADC

AMPLIFIER CHIP

8 - 32 channels

ANALOG
STORAGE-CHIP
(SAPE)

512 capacitors
per channel
32 channels/chip

Writing Speed
10 MHZ

Reading Speed
1-2 MHZ

ADC-CHIP

32 channels/chip
1-2 MHZ
8-bit
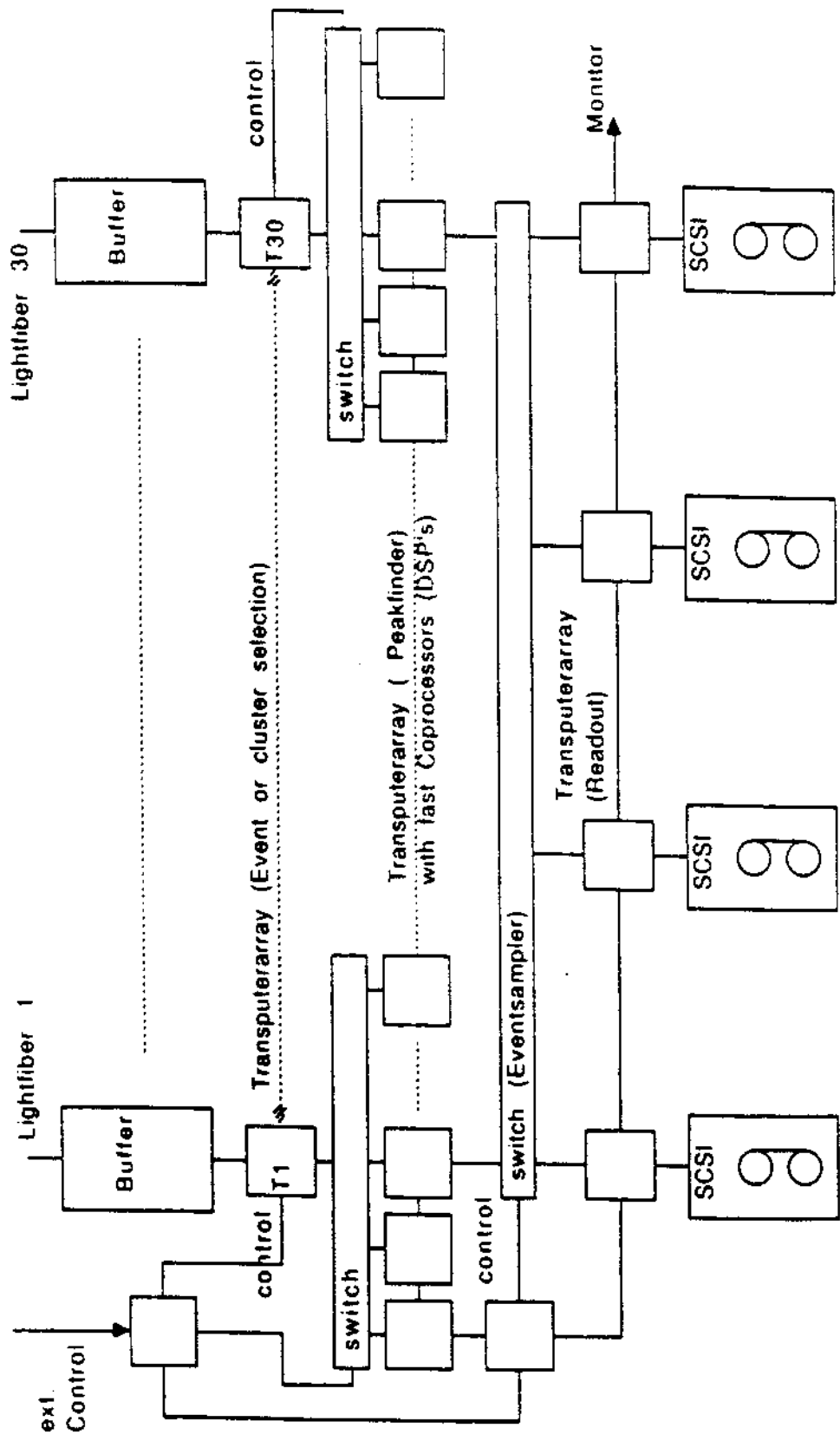Pipe line
ADC

Fig.22   TPC front end electronics

Fig. 2a

Conceptual layout for online data reduction and readout using an array of transputers.

This layout assumes, that the zero suppression is already done at the detector
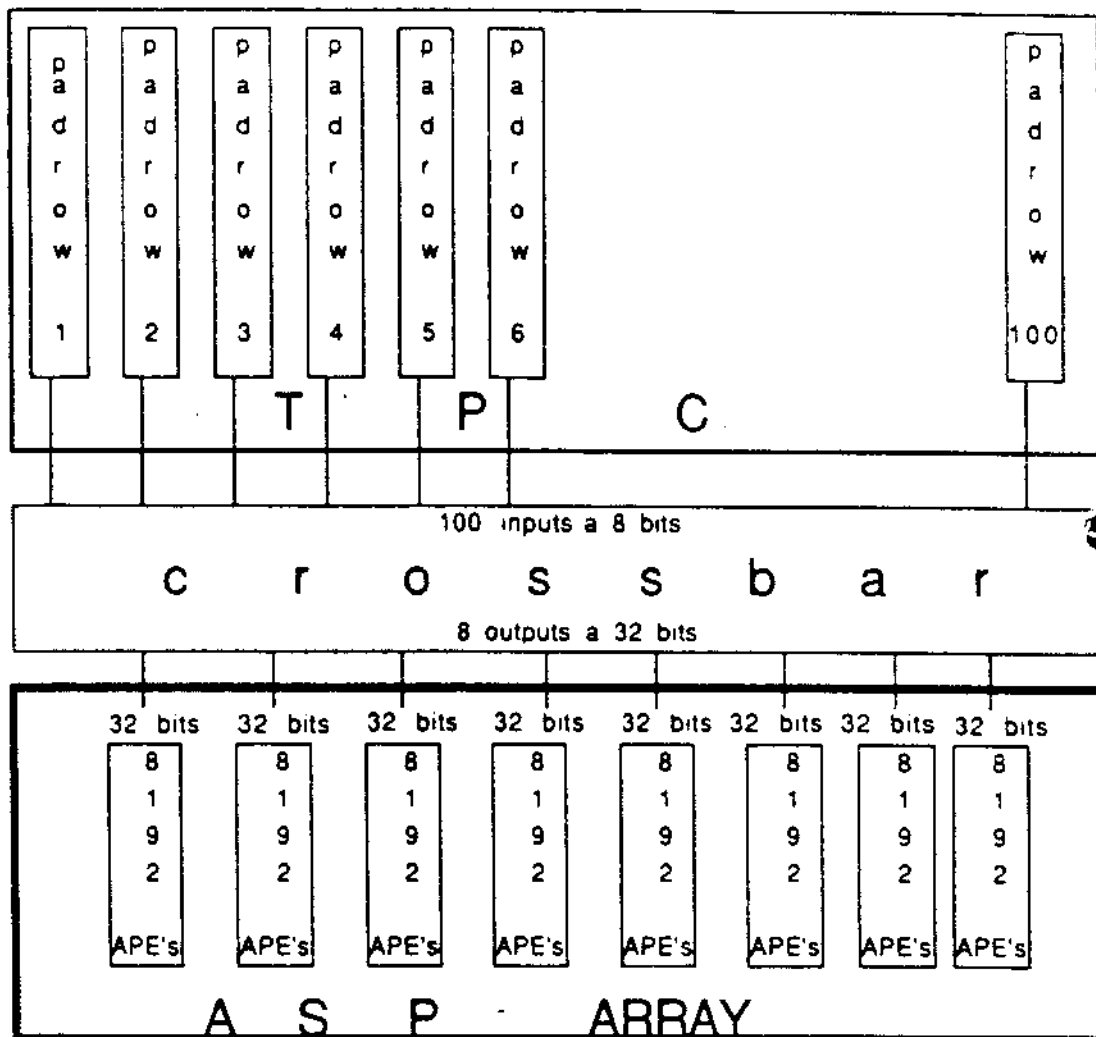
Fig. 24

Concept for online data reduction using an array of Associated String Processors (ASP's) arranged in 8 groups of Associated Processor Elements (APE's) each consisting out of 8192 ASP's.